Article

Not peer-reviewed version

Unravelling the Function of the Sesquiterpene Cyclase STC3 in the Life Cycle of *Botrytis cinerea*

Víctor Coca-Ruiz , Ivonne Suárez , Josefina Aleu , Jesús M. Cantoral , Celedonio González , Carlos Garrido , Nélida Brito * , and Isidro G. Collado *

Posted Date: 27 March 2024

doi: 10.20944/preprints202403.1652.v1

Keywords: *Botrytis cinerea*; sesquiterpene cyclase; secondary metabolism; metabolites and sesquiterpenes

Article

Unravelling the Function of the Sesquiterpene Cyclase STC3 in the Life Cycle of *Botrytis cinerea*

Víctor Coca-Ruiz [1,2,#], Ivonne Suárez [1,2,3,#], Josefina Aleu [1,2], Jesús Cantoral [3,4], Celedonio González [5], Carlos Garrido [3,4], Nélida Brito [5,*] and Isidro G. Collado [1,2,*]

[1] Departamento de Química Orgánica, Facultad de Ciencias, Universidad de Cádiz, 11510 Puerto Real, Cádiz, Spain.
[2] Instituto de Investigación en Biomoléculas (INBIO), Universidad de Cádiz, 11510 Puerto Real, Cádiz, Spain.
[3] Departamento de Biomedicina, Biotecnología y Salud Pública, Laboratorio de Microbiología, Facultad de Ciencias del Mar y Ambientales, Universidad de Cádiz, 11510, Puerto Real, Spain.
[4] Instituto de Investigación Vitivinícola y Agroalimentaria (IVAGRO), Universidad de Cádiz, 11510 Puerto Real, Cádiz, Spain.
[5] Área de Bioquímica y Biología Molecular, Departamento de Bioquímica, Microbiología, Biología Celular y Genética, Universidad de La Laguna, 38200 San Cristóbal de La Laguna, Tenerife, Spain
* Correspondence: nbrito@ull.edu.es (N.B.); isidro.gonzalez@uca.es (I.G.C.); Tel.:+34 922318356 (N.B.); Tel.: +34 956012768 (I.G.C.)
[#] These authors contributed equally to this work

Abstract: The genome sequencing of *Botrytis cinerea* has supplied a general overview of the map of genes involved in secondary metabolite synthesis. *B. cinerea* genomic data have revealed that this phytopathogenic fungus has seven sesquiterpene cyclase (*Bcstc*) genes that encode proteins involved in the farnesyl diphosphate cyclization. Three sesquiterpene cyclases (BcStc1, BcStc5 and BcStc7) have been characterized, related to the biosynthesis of botrydial, abscisic acid and (+)-4-epi-eremophilenol, respectively. However, the role of the other four sesquiterpene cyclases (BcStc2, BcStc3, BcStc4 and BcStc6) remains unknown. BcStc3 is a well-conserved protein with homologues in many fungal species, and here, we have undertaken its functional characterization in the life cycle of the fungus. A null mutant Δ*Bcstc3* and an overexpressed–*Bcstc3* transformant (Ov*Bcstc3*) were generated, and both strains show deregulation of those other sesquiterpene cyclase-encoding genes (*Bcstc1*, *Bcstc5*, *Bcstc7*). These results suggest a co-regulation of the expression of the sesquiterpene cyclase gene family in *B. cinerea*. Phenotypic characterization of both transformants revealed that BcStc3 is involved in oxidative stress tolerance, production of reactive oxygen species and virulence. The metabolomic analysis allowed the isolation of characteristic polyketides and eremophilenols from the secondary metabolism of *B. cinerea*, although no sesquiterpenes different from those already described were identified.

Keywords: *Botrytis cinerea*; sesquiterpene cyclase; secondary metabolism; metabolites and sesquiterpenes

1. Introduction

Sesquiterpenes are C15 terpenes consisting of three isoprene units, found in linear (as farnesene), monocyclic (as zingiberene and humulene), bicyclic (as caryophyllene), tricyclic (as longifolene), and tetracyclic (as punctaporonin C) forms. They are produced by higher plants, marine organisms and fungi [1–3]. The biological activity of many of these natural products is related to human health. For instance, arvestolides H and I, and artefreynic acids B, C, and G inhibit the production of nitric oxide [4,5]; chrysanthemulide A has anti-inflammatory activity [6]; 14-*O*-acetylinsulicolide A, 6β,9α-dihydroxy-14-*p*-nitrobenzoylcinnamolide and insulicolide A are cytotoxic against renal carcinoma cell lines [7], or santhemoidin A is active against *Trypanosoma brucei* rhodesiense trypomastigotes [8].

 doi:10.20944/preprints202403.1652.v1

Moreover, sesquiterpenes have been recognized as replacements for petroleum-derived jet-engine fuels [9]. These findings highlight the need to deepen the analysis of sesquiterpene biosynthesis due to their commercial interest.

The sesquiterpene synthases (EC:4.2.3.-) are a group of enzymes that convert the linear C15 precursor farnesyl diphosphate (FDP) into a diverse class of natural products. Many sesquiterpenes are cyclic compounds, and the first reaction in their biosynthesis is the cyclization of FDP at the proximal C6-C7 or the distal C10-C11 double bond. Therefore, the synthases involved in this step are also named sesquiterpene cyclases (STC) [10–13]. Subsequent modifications such as oxidations or substitution with different functional groups, a lactone ring and rearrangements of the 15-carbon skeleton produce the related sesquiterpenoids [14,15].

In fungi, these compounds constitute the most abundant and diverse group of all categories in the vast system of natural products [16]. Many act as phytotoxins in the interaction between phytopathogenic fungi [17,18] and their host [19]. Botrydial is one example of these non-host-specific toxic sesquiterpenes. It is produced by the phytopathogenic fungus *B. cinerea*, the causal agent of gray mold, classified as the second most relevant plant pathogen for its economic and scientific importance [20]. Botrydial is secreted during the fungus-host interaction, causing chlorosis and cell collapse, and its role in virulence is closely related to the polyketide botcinin, the second major phytotoxin of *Botrytis* [21,22]. It triggers the hypersensitive response of plants to pathogens, modulated by salicylic acid and jasmonic acid signaling, that produces a rapid localized cell death [23]. Botrydial also induces phosphatidic acid production, a phospholipid second messenger involved in the induction of plant defense responses [24]. Moreover, this phytotoxin also modulates the interaction of *B. cinerea* with other fungi and bacteria and their environment [25,26].

Over the last several years, our group has been studying the sesquiterpene synthesis by *B. cinerea* [27]. We found six *Bcstc* genes in the *B. cinerea* B05.10 strain (*Bcstc1* or *Bcbot2*, *Bcstc2*, *Bcstc3*, *Bcstc4*, *Bcstc5* or *Bcaba5*, and *Bcstc7*) that encode proteins with the two conserved magnesium binding sites required for FDP cyclization. A seventh *Bcstc* gene, *Bcstc6* (Gene ID BofuT4P10000109001), is specific to the T4 strain and absent in B05.10 [28]. We have functionally characterized the sesquiterpene cyclases BcStc1, BcStc5, and BcStc7. *Bcstc1* encodes for a pentalenene cyclase, which generates the tricyclic alcohol presilphiperfolan-8β-ol as a precursor of botrydial phytotoxins and other important derived sesquiterpenes [29,30]. On the other hand, BcSct5 is essential for the synthesis of the sesquiterpenoid abscisic acid [31–34], and BcStc7 is involved in (+)-4-epi-eremophilenol biosynthesis, a member of the family of eremophilene sesquiterpenes [35–37]. However, the biosynthesis of these two compounds is not fully understood yet [27]. The role of the three other sesquiterpene cyclases of *B. cinerea* is still unknown. To date, BcStc2, BcStc3 and BcStc4 remain uncharacterized.

Here, we achieve the functional characterization of the sesquiterpene cyclase 3 (BcStc3). We describe the *Bcstc3* expression pattern in vitro and *in planta* and investigate the putative role of the protein in the virulence and biology of *B. cinerea*, generating a *Bcstc3* knock-out mutant and a new strain that constitutively expresses the *Bcstc3* gene.

2. Results

2.1. BcStc3 is a Well Conserved Protein

BcStc3 has 411 amino acid residues with a theoretical molecular weight of 486551.89 g/mol and an isoelectric point of 6.34, estimated using the Expasy Protparam tool (https://web.expasy.org/protparam/). Its aliphatic index is predicted to be 90.73, and the grand average of hydropathicity (GRAVY) is -0.381, indicating that BcStc3 is a thermostable soluble protein, located in the cell cytoplasm, according to DeepLoc 2.0 (https://services.healthtech.dtu.dk/services/DeepLoc-2.0/) prediction. A terpene synthase family 2, C-terminal metal binding domain (Pfam 19086, at 170-336 amino acid residues) was identified using the InterProScan software [38] and as a terpene cyclase-nonplant C1 protein (cd00687, from 147 to 336 residue) according to Conserved Domain Database (CDD) from NCBI [39,40]. Both domains were also found in the BcStc1, BcSct4 and BcStc5 proteins (Table 1), but BcStc3 showed the highest sequence identity percentage with BcStc4 (23.84%). The other two members of the BcStc protein family of *B.*

 doi:10.20944/preprints202403.1652.v1

cinerea B05.10 (BcStc2 and BcStc7) are grouped into the trichodiene synthase or TRI5 family (Pfam 06330 domain), and the percentage identity values with the other four family proteins range between 11.21 to 20.66% (Table 1).

Table 1. BcStc protein family of *B. cinerea* B05.10.

gene ID[a]	Accession number[b]	protein name	% Identity[c]						aa	pfam[d]	Name[e]	EC number[e]	Reaction (IUBMB)[e]
Bcin12g06390	XP_024552383.1	BcStc1/BcBot2	100.00						399	PF19086	presilphiperfolanol synthase	4.2.3.74	(2*E*,6*E*)-farnesyl diphosphate + H_2O = presilphiperfolan-8β-ol + diphosphate
Bcin08g02350	XP_001551948.1	BcStc2	13.06	100.00					329	PF06330	trichodiene synthase	4.2.3.6	(2*E*,6*E*)-farnesyl diphosphate = trichodiene + diphosphate
Bcin13g05830	XP_024552712.1	BcStc3	14.28	15.80	100.00				411	PF19086	aristolochene synthase	4.2.3.9	(2*E*,6*E*)-farnesyl diphosphate = aristolochene + diphosphate
Bcin04g03550	XP_001546971.2	BcStc4	16.54	20.66	23.84	100.00			441	PF19086	ophiobolin F synthase	4.2.3.145	(2*E*,6*E*,10*E*,14*E*)-geranylfarnesyl diphosphate + H_2O = ophiobolin F + diphosphate
Bcin01g03520	XP_001550978.1	BcStc5	19.19	11.76	13.93	16.09	100.00		323	PF19086	fusicocca-2,10(14)-diene synthase	4.2.3.43	geranylgeranyl diphosphate = fusicocca-2,10(14)-diene + diphosphate
Bcin11g06510	XP_024551950.1	BcStc7	12.77	17.44	14.95	14.33	11.21	100.00	321	PF06330	trichodiene synthase	4.2.3.6	(2*E*,6*E*)-farnesyl diphosphate = trichodiene + diphosphate
			BcStc1/BcBot2	BcStc2	BcStc3	BcStc4	BcStc5	BcStc7					

[a] Gene ID from Ensembl Fungi data base (hpp://fungi.ensembl.org/). [b] Protein ID from on NCBI database (https://www.ncbi.nlm.nih.gov). [c] Sequence identities were obtained using Sequence Identity And Similarity online tool (SIAS – http://imed.med.ucm.es/Tools/sias.html). [d] Pfam domain signatures were found using the InterProScan software [38] and Conserved Domain Database (CDD) from NCBI [41]. [e] Protein sequences were annotated using KEGG BlastKoala annotation tool (KEGG Orthology and Links Annotation) [42].

The conservation profile of BcStc3 protein amino acid residues (Figure 1A) was predicted by the Con Surf web server (http://consurf.tau.ac.il), and the conservation score for each residue (Figure 1B) was calculated with Al2CO (**http://prodata.swmed.edu/al2co/al2co.php**) taking 200 homologous

 doi:10.20944/preprints202403.1652.v1

protein sequences obtained doing a BlastP [43] of the BcStc3 protein sequence with the criteria of >30% identity and >70% coverage. The results showed low conservation of residues in the N-terminal region, but different canonical motifs of the class I terpenoid cyclases [44,45] were identified at the C-terminus region (Figure 1B). The two conserved motifs involved in the binding of the magnesium cations were found: the aspartic-rich motif, DDMWE, at amino acid 177, and the NSE/DTE motif, NDLASYDKE, at amino acid 307 (Figure 1). Moreover, the conserved effector triad was identified at R264-D267-I268 (Figure 1), and the RY conserved pair related to the binding of farnesyl pyrophosphate [46,47] was located at the C-terminus of the protein (residues 401 and 402, respectively) (Figure 1). The molecular model of BcStc3 protein was generated using Alphafold [48], finding the α-helical fold (Figure 2) typical for class I terpene synthase [13,49]. As expected, the arrangement of the conserved motifs identified in the sequence defines the catalytic site of the protein (Figure 2). Furthermore, the H-α1 loop, a conserved structural motif that shields the active site and stabilizes the closed enzyme conformation after the substrate binding [50] and the conserved asparagine residue (N329) at the C-terminus of the H-1α loop were also identified in the BcStc3 model (Figure 2).

Preprints.org (www.preprints.org) | NOT PEER-REVIEWED | Posted: 27 March 2024 doi:10.20944/preprints202403.1652.v1

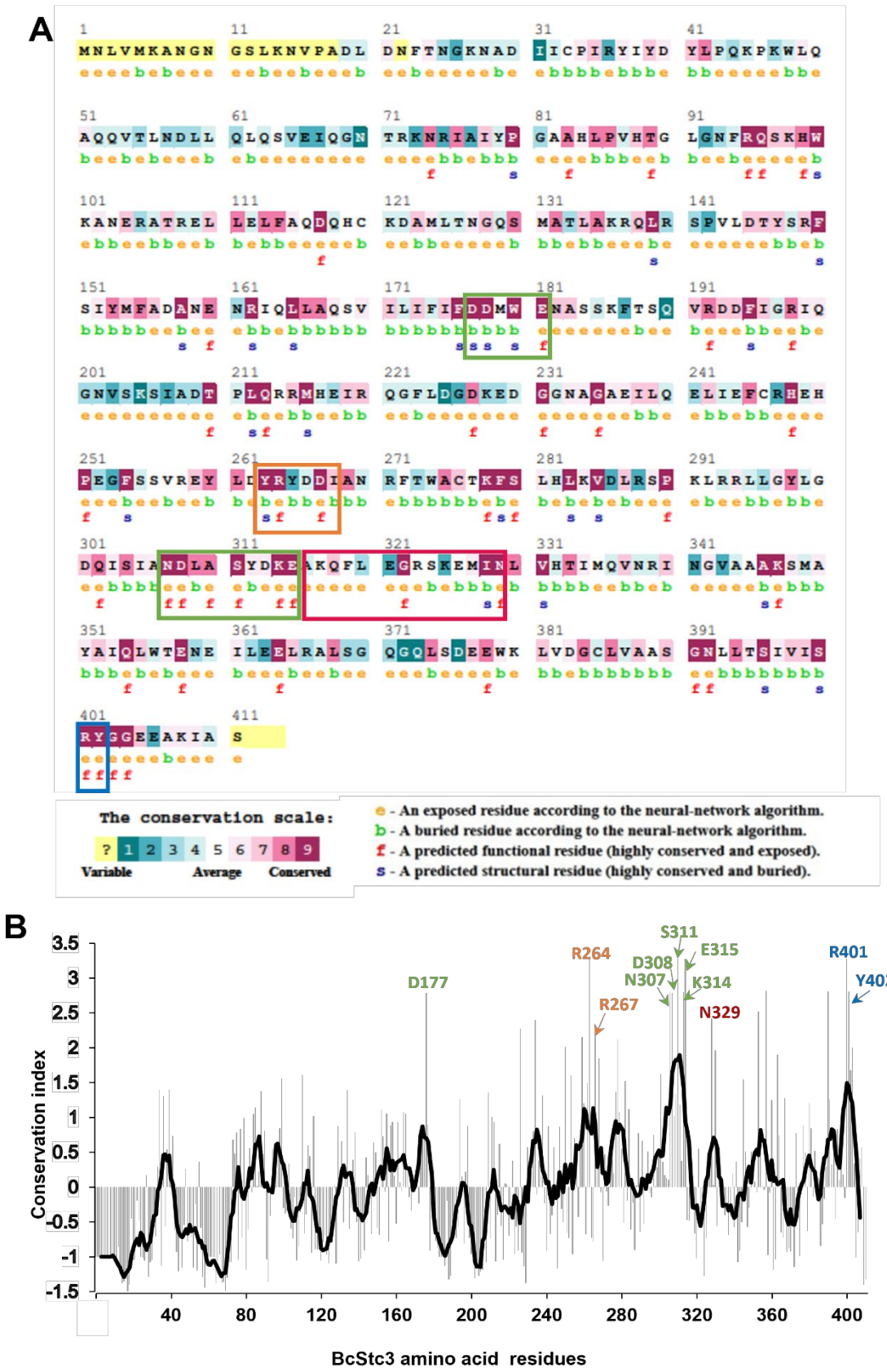

Figure 1. (A) The conservation pattern of the BcStc3 sequence calculated by Con Surf server. Amino acid residues are colored turquoise to bordeaux according to the conservation scores. Green boxes indicate the two conserved magnesium binding motifs. Orange box denotes conserved effector triad. Blue box indicates conserved R and Y residues involved in substrate binding. Red box indicates H1α-loop ending at the conserved asparagine (N329) residue. (B) Position-specific evolutionary

Preprints.org (www.preprints.org) | NOT PEER-REVIEWED | Posted: 27 March 2024 doi:10.20944/preprints202403.1652.v1

conservation scores of each residue of BcStc3. Scores were calculated with AL2CO (http://prodata.swmed.edu/al2co) for an alignment of 160 BcStc3-like proteins downloaded from NCBI and aligned with Clustal Omega (https://www.ebi.ac.uk/services). Conservation indexes were averaged in windows of seven residues to smooth the graph. The conserved residues of the canonical motifs of the class I terpenoid cyclases are indicated and colored according to the boxes in (A).

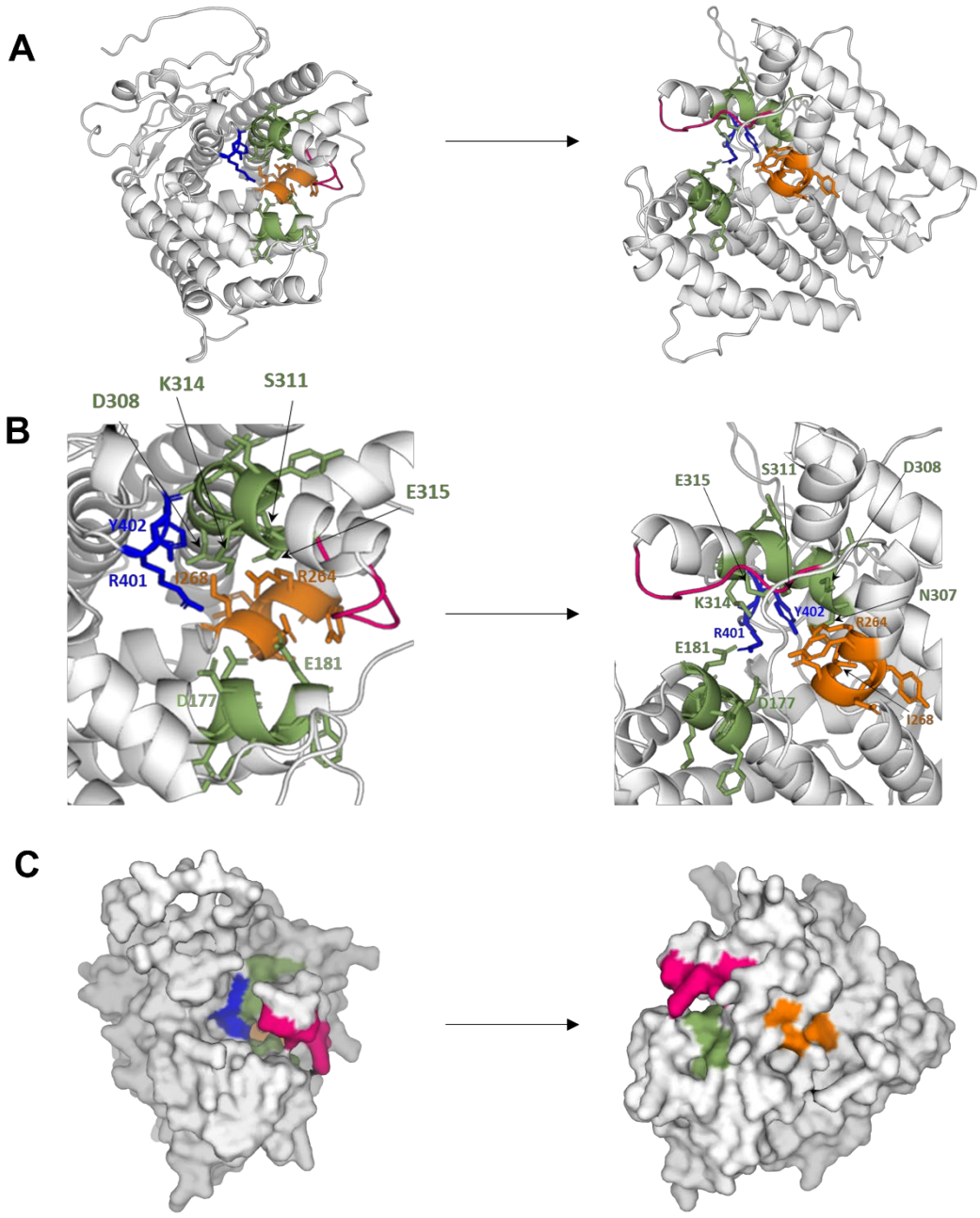

Figure 2. Tertiary structure of the protein BcStc3 via AlphaFold modelling. (A) Cartoon representations highlighting the two magnesium binding motifs (green), the effector triad (orange) and the H1α-loop (red). The R401 and Y402 residues, involved in substrate binding, are shown as sticks (blue). (B) Close-up view of the active site of BcStc3. The canonical conserved residues are shown as sticks. (C) Surface views of BcStc3; the conserved motifs are colored as in (A).

The putative conservation of BcStc3 in *Botrytis* species was analyzed. A BlastP search against the NCBI non-redundant protein sequences database restricted to the genera *Botrytis* (taxid: 33196) and *Botryotinia* (taxid: 40558) was performed using BcStc3 as a query sequence. The results showed that

 doi:10.20944/preprints202403.1652.v1

BcStc3 is a well-conserved protein (Supplementary Figure S1). Homologous proteins were found in *Botrytis tulipae*, *Botrytis sinoallii*, *Botrytis elliptica*, *Botrytis deweyae*, *Botrytis galanthina*, *Botrytis hyacinthi*, *Botrytis byssoidea*, *Botryotinia globosa*, and *Botryotinia narcissicola*, with a percent identity of over 80% and a query coverage exceeding 95%. The multiple sequence alignment showed that the functional motifs identified in BcStc3 are conserved, except in the XP_038737186.1 protein of *B. byssoidea*, which lacks the DDMWE motif due to an insertion of 30 amino acid residues at the first aspartic residue (Supplementary Figure S1). As a result, the percent identity of this protein (estimated using the SIAS software) with the rest decreased to approximately 40%, while the other proteins exhibited values greater than 90%. Additionally, the XP_038737186.1 protein was positioned on a distinct branch of the phylogenetic tree derived from the sequence alignment of the BcStc3 protein sequence with those of other *Botrytis* species, using the Neighbor-Joining method (Figure 3).

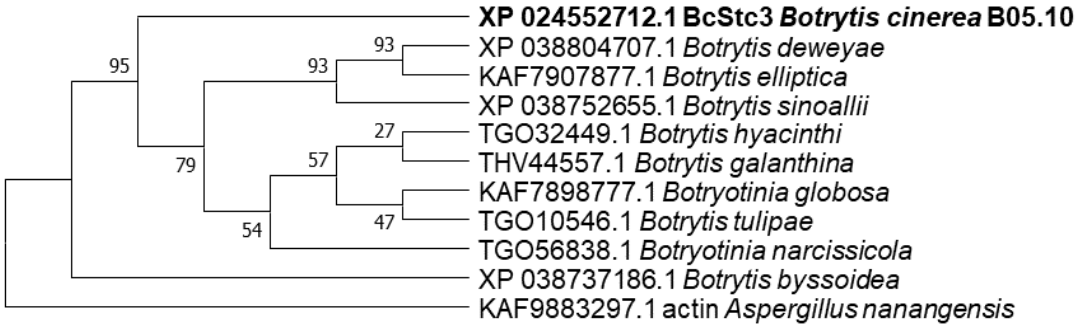

Figure 3. Phylogenetic tree of BcStc3 and homologous protein sequences of other *Botrytis* species. The phylogenetic tree was inferred using the Neighbor-Joining method via MEGA X software with bootstrap values for 1000 replicates are indicated. Protein sequences were selected after running similarity search by BlastP using BcStc3 as query sequence. NCBI accession number of each sequence is shown. Actin (KAF9883297.1) of *A. nanangensis* was used as outgroup.

A second BlastP search was conducted, this time excluding the *Botrytis* and *Botrytioinia* taxids. The results were filtered based on percent identity (>30%), coverage (>70%) and the bit-score (>50) according to [51], and 168 sequences fulfilled these criteria. Five multidomain proteins (ESZ93961.1, KAH7563860.1, KAF4304151.1, EKG18134.1, and XP_049153155.1) and three other proteins (XP_051299547.1, CAI6339174.1, and KAG7009610.1), lacking the PF19086 domain or being partial annotated, were removed from the analysis. The 160 remaining sequences were distributed in 124 organisms distributed in Dikarya fungi (Supplementary information Table S2). Seven proteins (1.5% of the total sequences) were annotated in three species of the Strophariaceae family (Agarycomycetes class, Basidiomycota) and the resting proteins were distributed in the Lectiomyceta (67.5%) and Sordariomyceta (28.1%) super-classes of Ascomycota (Table 2). Moreover, 60.6% of the total proteins were annotated in Eurotiomycetes and Dothideomycetes species (Table 2). Noteworthy is the absence of BcSTc3-like proteins in subphyla Taphrinomyctina and Saccharomycotina.

Table 2. Distribution of homologous proteins to Bcstc3 in the Kingdom Fungi.

Phylum	Sub-phylum	Super-class	Fungal-class	Number of proteins	Number of organisms
Ascomycota	Pezizomycotina	Leotiomyceta	Candelariomycetes	1	1
			Lecanoromycetes	9	9
			Eurotiomycetes	57	40
			Xylobotryomycetes	1	1

 doi:10.20944/preprints202403.1652.v1

		Dothideomycetes	40	27
	Sordariomyceta	Leotiomycetes	11	11
		Sordariomycetes	34	32
Basidiomycota	Agaricomycotina	Agaricomycetes	7	3

The alignment of the first 55 sequences retrieved from the BlastP search was used to construct a phylogenetic tree. Two clades were identified (Figure 4). Clade I includes most of the BcStc3-homologous proteins annotated in the Sordariomycetes fungi together with sequences from Eurotiales (Eurotiomycetes) and Pleorales (Dothideomycetes) organisms (Figure 4). Clade II consists of two groups. One is made up of BcStc3-related proteins from Botryosphaeriales (Dothideomycetes incertae sedis) and Helotiales (Leotiomycetes) fungi and the only member of Xylobotryomycetes class (Figure 4). The BcStc3 falls into the second group, clustered together with the PQE05643.1 protein of *Rutstroemia* sp. (Helotiales, Leotiomycetes) and the KAI9816264.1 protein of *Pycnora praestabilis*, the only member of the Candelariomycetes class (Figure 4). All the proteins of Lecanoromycetes fungi, and one of the seven BcStc3-like proteins found in Basidiomycota (the KDR73888.1 protein of *Galerina marginata*) were also clustered in this second group (Figure 4).

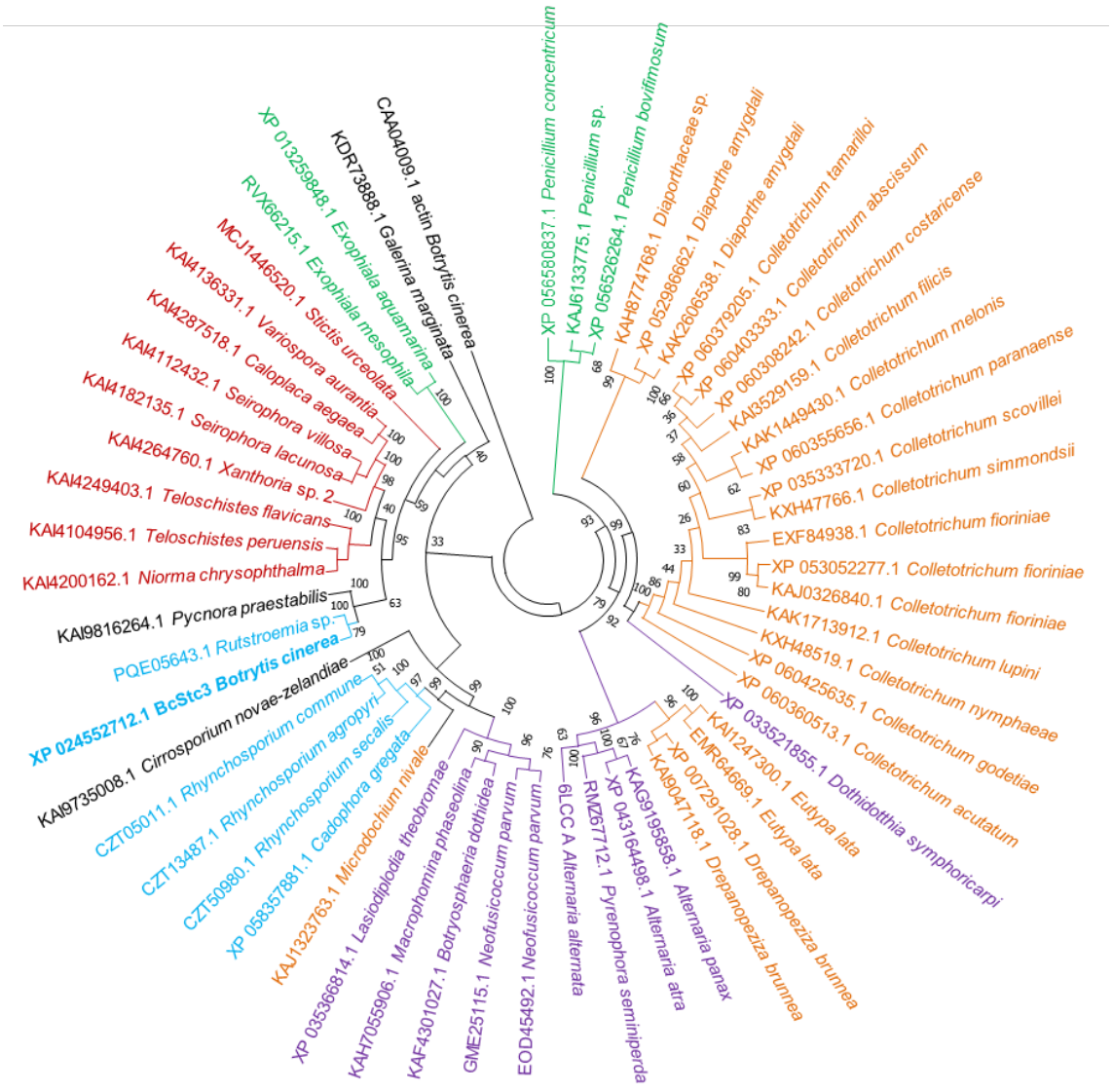

 doi:10.20944/preprints202403.1652.v1

Figure 4. Phylogenetic tree of BcStc3 and homologous protein sequences of other fungi species. The phylogenetic tree was inferred using the Neighbor-Joining method via MEGA X software and bootstrap values from 1000 trials are indicated at each branch node. Protein sequences were selected after running similarity search by BlastP using BcStc3 as query sequence, excluding the *Botrytis* and *Botryotinia* taxids (33196 and 40558, respectively), and filtering the results based on percent identity >30%, coverage >70% and the bit-score >50. The top 55 hits were retrieved for sequence alignment and phylogenetic analysis. NCBI accession number of each sequence is shown. Actin (CAA04009.1) of *B. cinerea* was used as outgroup. Taxonomic distribution is highlighted by different colors: Eurotiomycetes (green), Sordariomycetes (orange), Dothideomycetes (violet), Leotiomycetes (blue), and Lecanoromycetes (red). The only members of the Xylobotryomycetes, Candelariomycetes, and Agaricomycetes (Basidiomycota) classes are highlighted in black.

2.2. Expression Analysis of the Sesquiterpene Cyclase Gene Family in B. cinerea

The basal expression of the sesquiterpene cyclase gene family in non-germinated conidia of the UCA992 strain was analysed by qRT-PCR. Results were normalized to *actA* and *B-tub* genes and depicted as fold-change relative to the lowest expressed gene (*Bcstc2*). All family genes were expressed in non-germinated conidia, being the *Bcstc5* transcripts the most abundant (approximately 30 times compared with that of *Bcstc2*), and *Bcstc3* and *Bcstc4* reaching transcript levels similar to the reference gene (Figure 5A). The *Bcstc5* gene was also the highest expressed gene in the non-germinated conidia of the B05.10 strain, but the *Bcstc*1 mRNAs were the least abundant transcripts, and the *Bcs*tc2 and *Bcst3* genes were expressed almost 8-times more than the *Bcstc1* gene (Supplementary Figure S2.A).

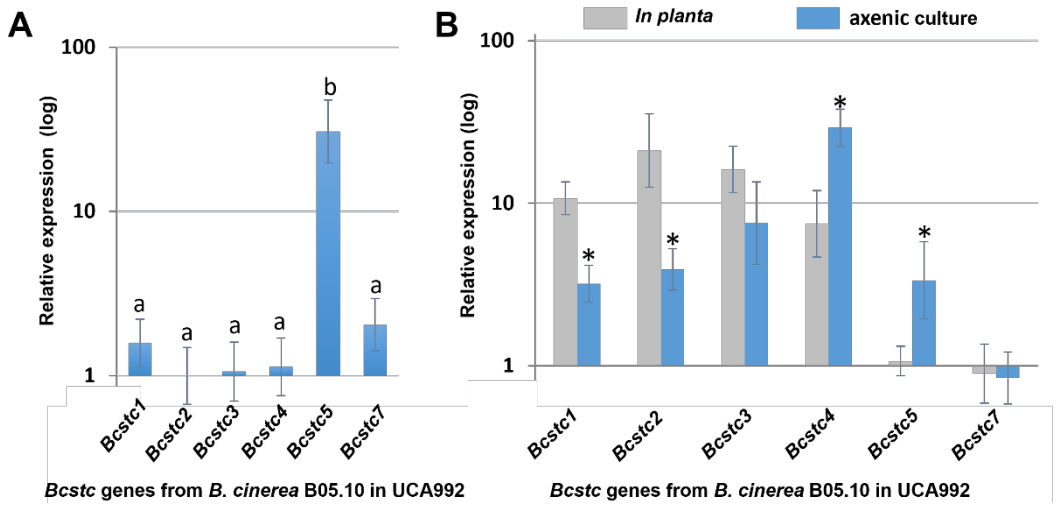

Figure 5. Gene expression of the *Bcstc* gene family in the *B. cinerea* UCA922 strain. (A) Relative expression levels of the *Bcstc* genes in ungerminated conidia. mRNA levels were quantified by qRT-PCR and normalized to *actA* and *B-tub* expression. Data are plotted as relative expression, compared to the *Bcstc2* expression level, set as 1. (B) Relative expression levels of the *Bcstc* genes in axenic culture and in planta. mRNA levels were quantified by qRT-PCR in mycelium grown in YGG medium for 96 hours (axenic culture) and in infected tissue of *Nicotiana tabaccum* leaves 96 hours post-inoculation with a conidial suspension (in planta). Values were normalized to *actA* and *B-tub* genes expression and data are plotted as relative expression, compared to the expression level of each gene in ungerminated conidia. Error bars show standard deviation of three biological replicates (n=3). Different letters above the bars in A mean that there are significant differences between genes with a p-value<0.05. * in B means the existence of significant differences between axenic and in planta culture for each gene with a p-value<0.05.

To evaluate the role of the sesquiterpene cyclases in the vegetative growth of *B. cinerea*, the expression pattern of the six *Bcstc* genes was examined at 96 hours after conidial germination in the

 doi:10.20944/preprints202403.1652.v1

YGG medium (Figure 5B). All genes were up-regulated related to the basal expression levels of each gene in non-germinated conidia (from 3 times for *Bcstc1* to almost 30 times for *Bcstc*4), except the *Bcstc7* gene, which hardly changed its expression (Figure 5B). Surprisingly, an increase of about 2000-fold in the *Bcsct7* mRNA levels was observed for the B05.10 strain at the same growth conditions (Supplementary Figure S2.B).

The *Bcstc3*, *Bcstc4*, *Bcstc1*, and *Bcstc2* genes were overexpressed after 96 hours of inoculating tobacco leaves with conidia of the UCA922 strain, especially *Bcstc2* and *Bcstc3* which increased 16 and 21 times, respectively, the mRNA levels related to non-germinated conidia (Figure 5B). However, the *Bcstc5* gene was not induced during the host-plant interaction (Figure 5B). Contrary, the *Bcstc1* and *Bcstc7* genes were significantly up-regulated *in planta* (almost 700 times respect to their basal level in non-germinated conidia) when tobacco leaves were inoculated with the B05.10 strain (Supplementary Figure S2.B).

2.3. Co-Regulation of Sesquiterpene Cyclase Genes in B. cinerea

The generation of the *ΔBcstc3* strain and the overexpressed-*Bcstc*3 transformant (Ov*Bcstc*3) allowed us to analyze the possible co-regulation of the *Bcstc* gene family. The *Bcstc3* gene deletion or its overexpression caused significant but different changes in the expression pattern of the gene family in non-germinated conidia (Figure 6A). The *Bcstc3* mutation induced the upregulation of the *Bcstc1*, *Bcstc2*, and *Bcstc4* genes, but especially of *Bcstc7* (over 40-fold changes) related to their expression levels in conidia of the wild-type strain (Figure 6A). However, the relative mRNA transcript levels of *Bcstc5* did not change (Figure 6A). On the other hand, the conidia of the Ov*Bcstc3* strain overexpressed the *Bcsct*5 gene (25-fold) and, to a lesser extent, the *Bcstc*7 and *Bcstc*2 genes (7.8 and 6.4-fold, respectively) with respect to the relative abundance of each transcript in conidia of the wild type strain (Figure 6A).

During fungal vegetative growth, the deletion and the overexpression of the *Bcstc3* gene also caused changes in the expression pattern of the gene family. After 96 hours in axenic culture, the transcript levels of the *Bcstc4*, *Bcstc5*, and, especially, *Bcstc*7 (24-fold) genes were higher in the mycelia of the *ΔBcsc*t3 and Ov*Bcstc*3 strains than in the wild type (Figure 6B). However, the expression level of *Bcstc1* hardly changed, and differential expression of *Bcstc*2 was observed in both modified strains (Figure 6B).

Changes in *Bcstc* gene family expression during fungus-plant interaction were quite different in the *Bcsct3* knock-out and the *Bcsct3* overexpressing strains. The *Bcstc3* deletion induced the up-regulation of the rest of the genes, especially of *Bcstc1* and *Bcsct7* (increasing the transcripts levels to 40 and 10 times, respectively, related to the parental strain) (Figure 6C). However, the *Bcsct1* gene expression almost did not change in the Ov*Bcstc3* strain (Figure 6C). On the contrary, the overexpression of the *Bcstc3* gene caused a significant increase of the *Bcstc5* mRNA levels (up to 107 times related to the wild-type strain) while only 2.3 times in the mutant strain (Figure 6C).

 doi:10.20944/preprints202403.1652.v1

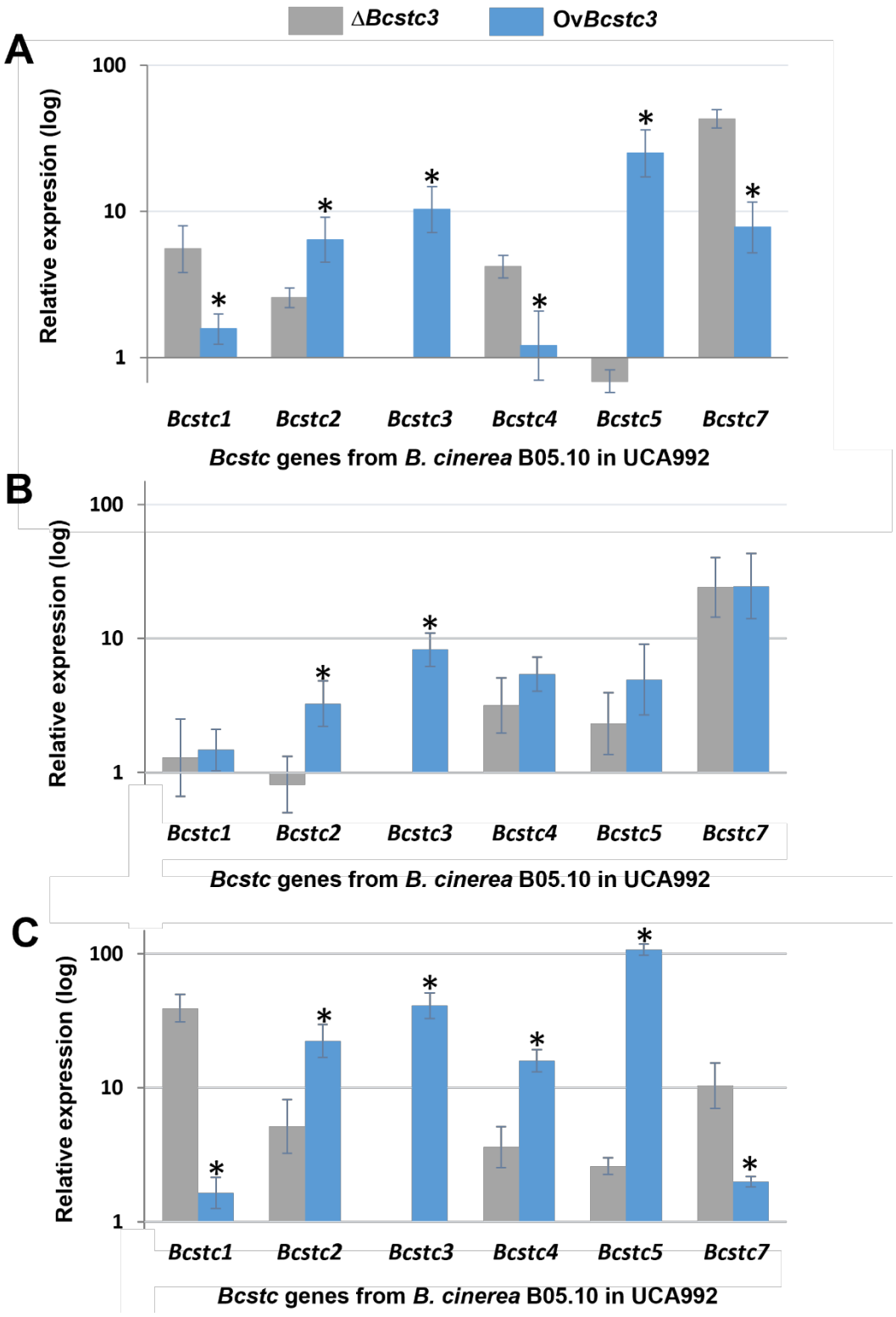

Figure 6. Gene expression of the *Bstc* gene family in the Δ*Bcstc3* and Ov*Bcstc3* strains. (A) Relative expression levels of the *Bcstc* genes in ungerminated conidia. mRNA levels were quantified by qRT-PCR and normalized to *actA* and *B-tub* expression. Data are plotted as relative expression compared to the expression level of each gene in ungerminated conidia of the *B. cinerea* UCA922 strain, set as 1. (B) Relative expression levels of the *Bcstc* genes in axenic culture. mRNA levels were quantified by qRT-PCR in mycelium grown in YGG medium for 96 hours (axenic culture). Values were normalized to *actA* and *B-tub* genes expression and data are plotted as relative expression, compared to the expression level of each gene of the *B. cinerea* UCA922 strain grown in the same conditions, set as 1. (C) Relative expression levels of the *Bcstc* genes *in planta*. mRNA levels were quantified by qRT-PCR

 doi:10.20944/preprints202403.1652.v1

in infected tissue of *N. tabaccum* leaves 96 hours post-inoculation with a conidial suspension of each strain. Values were normalized to *actA* and *B-tub* genes expression and data are plotted as relative expression, compared to the expression level of each gene in of the *B. cinerea* UCA922 strain at the same infection conditions. Error bars show standard deviation of three biological replicates (n = 3). * in A, B and C means the existence of significant differences between Δ*Bcstc3* and Ov*Bcstc3* for each *Bcstc* gene in each condition (A, B or C) with a *p*-value<0.05.

2.4. BcStc3 is Related to Fungal Growth and Stress Responses

The potential role of BcStc3 in fungal development was investigated by comparing the growth of the Δ*Bcstc3* and Ov*Bcstc3* transformants with that of the wild-type strain in solid and liquid YGG media. After four days of growth on YGG agar, the colony radius of both transformants decreased by approximately 14% (Figure 7A), with similar results observed in the estimated growth rate of the colony radius (Figure 7B). In liquid culture, however, the mycelial fresh weight and fungal biomass were only reduced in the Ov*Bcstc3* strain, exhibiting decreases of 15% and 22%, respectively, compared to the UCA922 strain (Figure 7C,D).

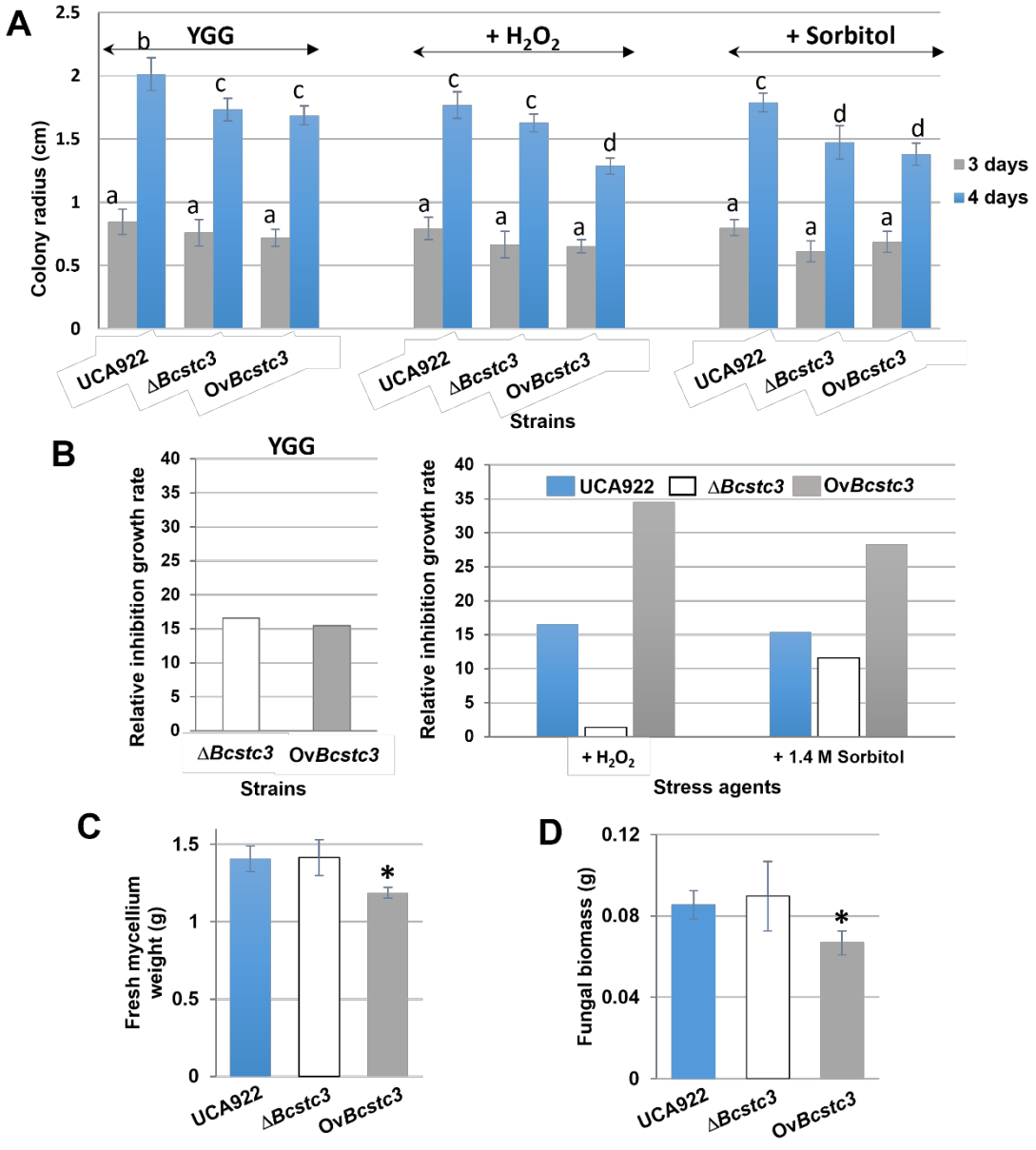

 doi:10.20944/preprints202403.1652.v1

Figure 7. BcStc3 is involved in fungal growth and tolerance to stress agents. (A) Colony radius of the indicated strains grown in YGG medium (YGG) and YGG supplemented with 1.5 mM hydrogen peroxide (+H_2O_2) or 1.4 M sorbitol (+sorbitol) after 3 and 4 days on incubation at 20˚C. The results are presented as the mean value ± standard deviation of fifteen biological replicates (n = 15). (B) Relative growth inhibition rate of the Δ*Bcstc3* and Ov*Bcstc3* strains grown in YGG solid medium, with respect to the UCA922 strain (YGG), and the relative growth inhibition rates of the three fungal strains grown in YGG solid medium supplemented with 1.5 mM hydrogen peroxide (+H_2O_2) or 1.4 M sorbitol (+1.4 M sorbitol), compared to the growth of each strain in the same medium without the stress agents. (D) Fresh mycelium weight and (E) fungal biomass of the indicated strains after fungal growth in YGG liquid medium for 96 hours at 20˚C (n=3 biological replicates). Statistical significance is denoted by different letter above the bars in A (p <0.05). * in C and D means statistical significance between UCA992 and Δ*Bcstc3* or Ov*Bcstc3* strains.

The impact of deleting or constitutively expressing the *Bcstc3* gene on fungal tolerance to osmotic and oxidative stresses was investigated by cultivating the strains on YGG plates supplemented with 1.4 M sorbitol or 1.5 mM hydrogen peroxide. Compared to the wild type, the Δ*Bcstc3* strain exhibited a reduction in colony radius of approximately 8% or 17% in media supplemented with peroxide or sorbitol, respectively (Figure 7A). However, both stress agents caused approximately a 25% reduction in the colony radius of the Ov*BcStc3* strain (Figure 7A).

The effect of sorbitol and hydrogen peroxide on the growth of each strain was evaluated by determining the relative inhibition growth rate, which involved calculating the changes in the colony growth rate for each strain in the presence of each of these agents compared to their growth rate in their absence. The results showed that hydrogen peroxide barely modified the growth rate of the mutant, whereas that of the Ov*Bcstc3* transformant decreased by 34.5% (Figure 7B). The growth rate of the UCA992 strain in the presence of peroxide decreased by 16.6% (Figure 7B), indicating that the deletion or overexpression of the *Bcstc3* gene modifies the fungal sensitivity to oxidative stress. On the other hand, the presence of sorbitol in the culture medium led to a reduction in the growth rate of 11.6% and 28.3% in the Δ*Bcstc3* and the Ov*Bcstc3* strains, respectively, while in the case of the wild type, the reduction was 15.4% (Figure 7B). These results also suggest the involvement of BcStc3 in osmotic stress tolerance.

2.5. BcStc3 is Involved in Virulence

To study the role of BcStc3 in fungal virulence, tomatoes, grapefruits, gerbera petals and detached tobacco leaves were inoculated with conidial suspensions of the wild type, Δ*Bcstc3* and Ov*Bcstc3* strains. The Δ*Bcstc3* displayed increased virulence in all the tested hosts compared to the wild type. The disease index in tomatoes and grapefruits increased by 18% and 12%, respectively, compared to the wild-type strain at four days post-inoculation (dpi) (Figure 8A,B, Supplementary Figures S3.A and S3.B). Also, the mean length of the lesions produced by the Δ*Bcstc3* on gerbera petals was 1.6-fold greater than those produced by the UCA922 strain at four dpi (Figure 8C, Supplementary Figure S3.C), and the lesions grew two times faster compared to the control (Figure 8D,). Finally, the mean diameter of the lesions caused by the mutant strain in tobacco leaves at four dpi and the lesion growth rate were also two times greater than those of the control (Figure 8E and 8F, Supplementary Figure S3.D).

The disease index of Ov*Bstc3*-inoculated tomato fruits slightly and gradually decreased over time by 10.3% compared to the wild-type strain four days after inoculation (Figure 8A, Supplementary Figure S3.A). However, there were no discernible differences between grapefruits infected by this transformant or the UCA922 strain (Figure 8B, Supplementary Figure S3.B). The growth rate of the lesions produced by the Ov*Bcstc3* strain in gerbera petals was only 5% lower than the control, but the mean size of the lesions at 2 and 3 days post inoculation were 38% and 22%, respectively, smaller than those produced by the wild-type strain (Figure 8C, Supplementary Figure S3.C). On the other hand, no significant differences were found in the virulence of Ov*Bcstc3* and UCA922 strains when tobacco leaves were inoculated (Figure 8E,F, Supplementary Figure S3.D).

 doi:10.20944/preprints202403.1652.v1

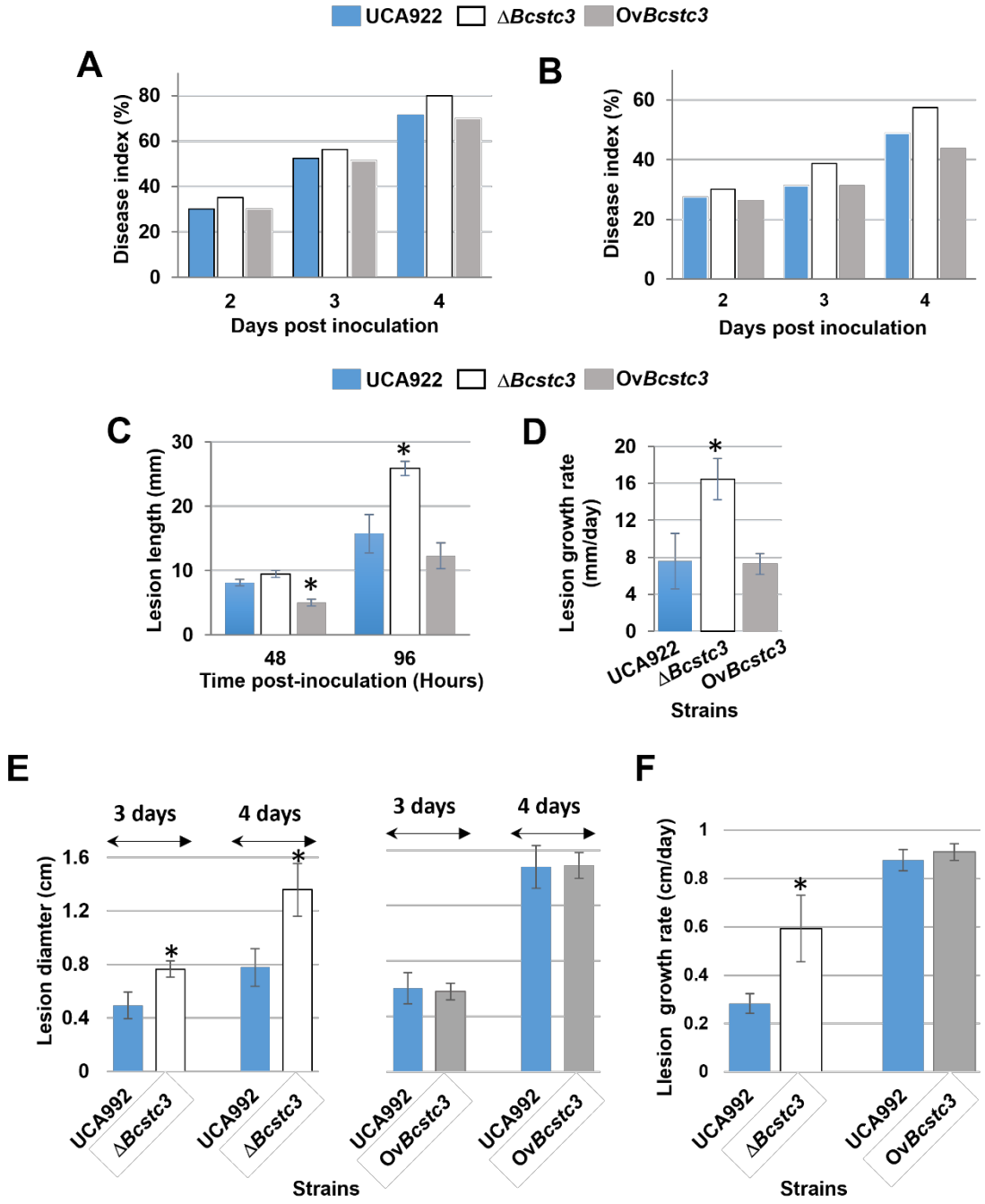

Figure 8. Deletion of the *Bcstc3* gene leads to increased virulence of *B. cinerea*. Different hosts were inoculated with 5 µL droplets containing 2500 conidia of the indicated strain in TGGK solution, incubated in the dark at 20°C under high humidity conditions and the degree of damage was estimated. (A) Disease index (%) of tomato fruits at 2-, 3- and 4-days post inoculation estimated with a qualitative scale (Supplementary Figure S3.A). (B) Disease index (%) of grapefruits at 2-, 3- and 4-days post inoculation estimated with a qualitative scale (Supplementary Figure S3.B). (C) Length and (D) growth rate (mm/day) of the lesions produced in gerbera petals estimated at days 3 and 4 after inoculation. (E) Diameter and (F) growth rate (cm/day) of the lesions produced in detached tobacco leaves 3- and 4-days post-inoculation. Fruit decay in tomatoes and grapefruits was determined for more than 30 fruits per fungal strain. The total number of inoculations on gerbera petals and tobacco leaves was greater than 15 per fungal strain and the results show the mean values ± SD. * means statistical significance between UCA992 and Δ*Bcstc3* or Ov*Bcstc3* strains.

2.6. BcStc3 is Involved in the Germination and Morphology of Conidia

 doi:10.20944/preprints202403.1652.v1

The production of conidia was assessed after growth on a solid tomato extract medium for ten days of incubation at 20°C, and the results showed no significant difference between the control and transformants (Figure 9A). However, the conidial area of the Ov*Bcstc3* strain was almost twice that of the wild type (Figure 9B). The percentage of aggregated conidia (assessed by counting conidial clustered in groups of two or more and by estimating the conidial sedimentation rate) increased by 38% in the conidia produced by the mutant and decreased by 38% in those produced by the Ov*Bcstc3* strain compared to the wild type (Figure 9C). Also, an opposite effect of deletion or constitutive expression of the *Bcstc3* gene on conidial germination was observed (Figure 9D). The conidial germination rate of the *ΔBcstc3* strain decreased by more than 50% compared to the wild-type strain, while an increase of approximately 17% was observed for the Ov*Bcstc3* strain (Figure 9D).

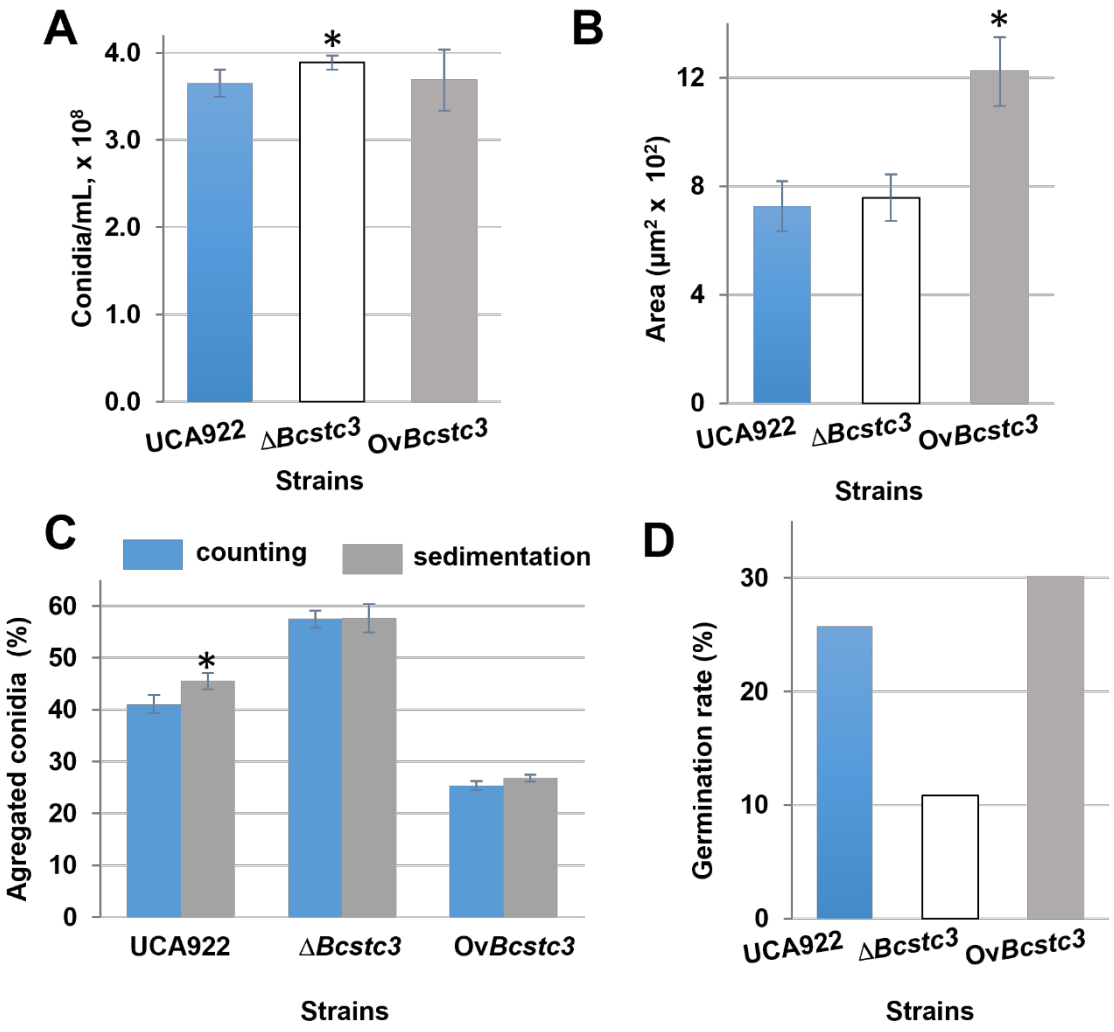

Figure 9. Involvement of BcStc3 in conidial morphogenesis and germination. (A) Conidial production of the indicated strain in tomato agar plates inoculated with agar plugs containing young mycelium exposed for 16 h to near-UV light three inoculation and incubated at 20°C for seven more days. (B) Bright-field pictures of conidia were taken with an Olympus BX-50 microscope and were used to measure the conidial area with the ImageJ software (n>100). (C) The percentage of conidia clustered in groups of two or more was calculated from random bright-field pictures of 10000 conidia in YGG incubated on a sterile glass slide for 6 hours at 20°C (counting), and the conidial sedimentation out of the suspension was estimated calculating the percentage of conidia that sediment after 2 hours at room temperature (sedimentation). (D) Conidial germination rate was calculated taking bright-field pictures of conidia incubated in YGG medium for 6 hours with the microscope and counting conidia with elongating germ tube longer than the conidial longitudinal diameter (germinated conidia) and

 doi:10.20944/preprints202403.1652.v1

expressed as percentage to the total conidia counted (n>100). * means statistical significance between UCA992 and Δ*Bcstc3* or Ov*Bcstc3* strains.

2.7. Bcstc3 Gene is Involved in ROS and Infection Cushion Production

The BcStc3 protein seems involved in the fungal response to oxidative stress. Therefore, the production of reactive oxygen species (ROS) was studied under different growth conditions. In axenic culture, the Ov*Bcstc3* strain released nearly double the amount of ROS into the medium compared to the wild type, while the *Bcstc3* deletion did not affect the ROS generation (Figure 10A). *In planta*, the infiltration of a DAB solution in tobacco leaves 48 hours after plant conidial inoculation revealed that the Δ*Bcstc3* strain produced nearly twice the amount of hydrogen peroxide in the lesion areas compared to the wild-type and Ov*Bcstc3* strains (Figure 10B).

On the other hand, as ROS is accumulated in the infection cushions [52], the production of these infection structures was assessed in the three fungal strains in axenic culture conditions. The results showed that the Ov*Bstc3* strain produced more infection cushions than the wild-type, while no change was observed for the *Bcsct3* null mutant (Figure 10C).

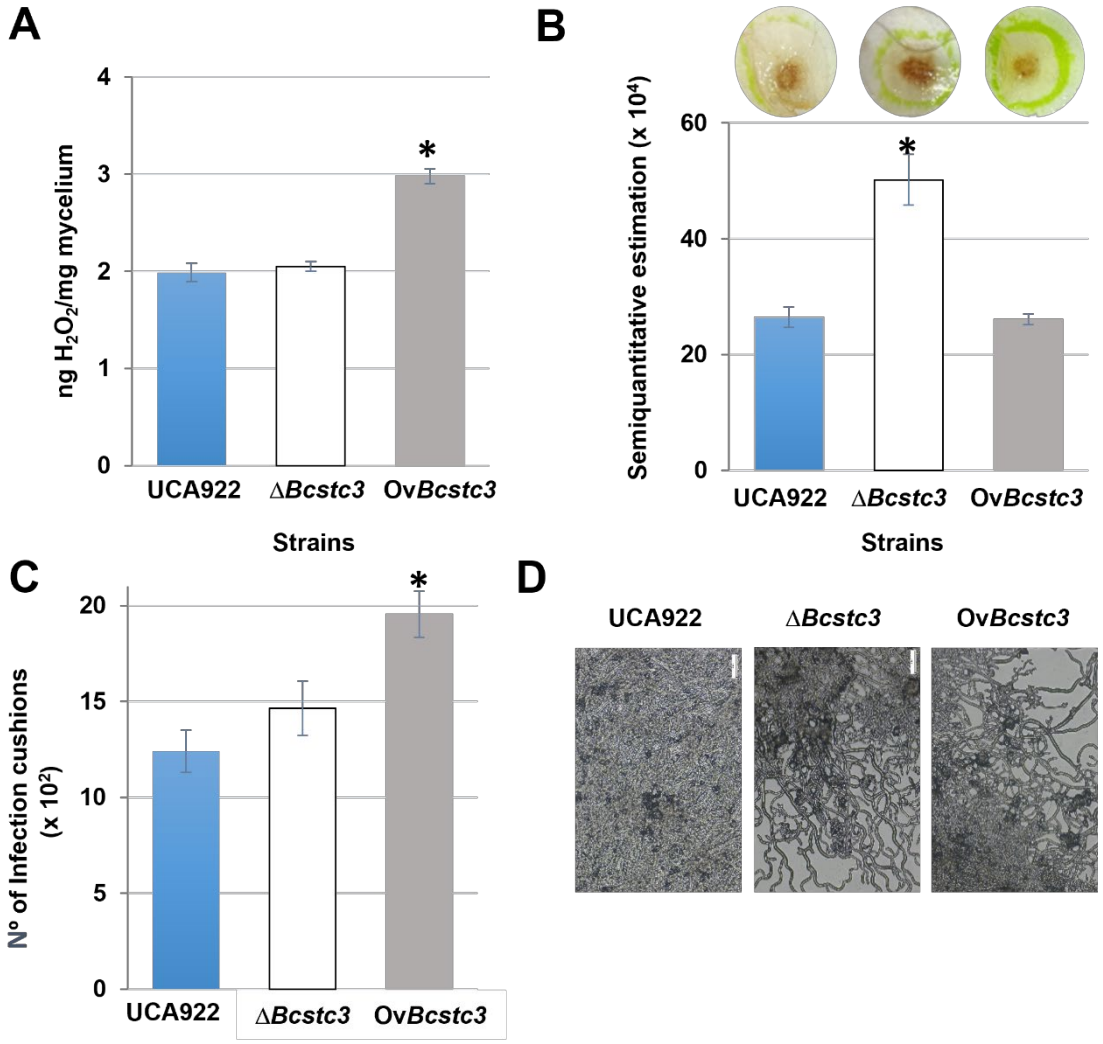

Figure 10. ROS production and BcStc3 are related. (A) ROS production in axenic culture by the indicated fungal strain incubating 24 mg of fresh mycelium with 1 mL of DAB solution for 5 hours and measuring the absorbance at 417 nm after discarded the mycelium. (B) ROS production in the infected area of tobacco leaves by the indicated fungal strain 48 after inoculation and vacuum infiltrated for 1 hour with 1 mg/mL DAB solution. ROS production was measured by ImageJ software, and values were expressed as the percentage of brown pixels detected around the infection point. (C)

 doi:10.20944/preprints202403.1652.v1

Infection cushion production on ¼ PDA plates after 48 hours of incubation at 20˚C and quantified following the semiquantitative method described by [42]. (D) Pictures representative of the infection cushions of (C). * Means statistical significance between UCA992 and Δ*Bcstc3* or Ov*Bcstc3* strains.

2.8. Implication of the BcStc3 on the Secondary Metabolism

The mutants were grown on malt agar medium to produce mycelium plugs which were further used to inoculate 40 Roux culture bottles, each containing 150 mL of modified Czapek-Dox medium. Bottles inoculated with six mycelium plugs were incubated for 27 days at 25°C.

The culture media (6 L), from each of the mutant strains, were filtered and the filtrates subjected to liquid-liquid extraction with ethyl acetate and dried over anhydrous sodium sulfate (see experimental for detailed procedures). Evaporation of the solvents yielded crude extracts as yellow oils, 173 mg (*ΔBcstc3*) and 153 mg (Ov*Bcstc3*).

The crude extracts were preliminary fractionated by column chromatography on silica gel eluting with *n*-hexane-EtOAc mixtures containing increasing percentages of EtOAc (9:1-0:10). The different fractions of interest were purified by semi-preparative HPLC with a mixture of *n*-hexane-EtOAc-acetone, (7:2:1) as the mobile phase and flow rate 2.5 mL/min. The isolated metabolites (Figure 11) were characterized by extensive spectroscopic and spectrometric mass analyses.

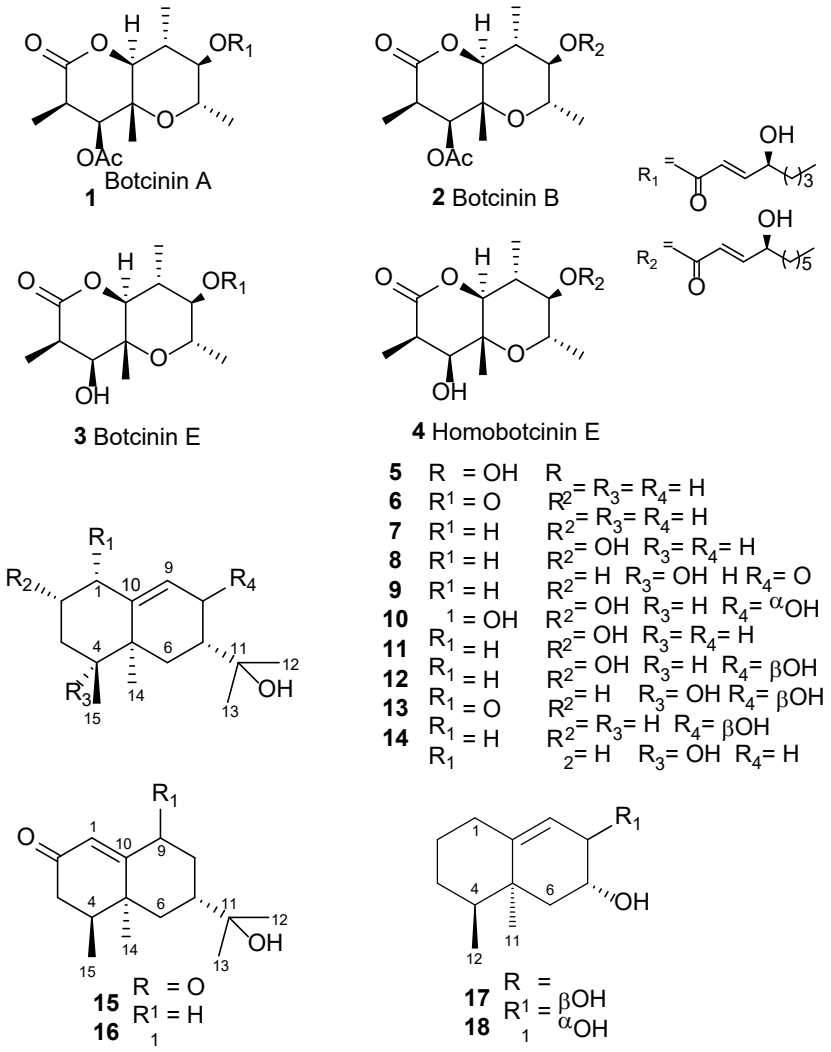

Figure 11. Secondary metabolites isolated from the fermentation of the *ΔBcstc3* or Ov*Bcstc3* strains.

The metabolomic analysis of the null mutant Δ*Bcstc3* broth yielded the polyketide derivatives **1** (1.8 mg), **2** (2.2 mg) and **3** (1.5 mg) [53], the known eremophil-9-en-11-ols **5** (6.5 mg), **6** (0.5 mg), **7** (3.0

 doi:10.20944/preprints202403.1652.v1

mg), **8** (3.0 mg), **9** (1.3 mg), **10** (2.0 mg), **11** (2.8 mg), **12** (0.8 mg), **13** (0.8 mg) and **14** (0.7 mg) [36,54], the 11-hydroxyeremophil-1(10)-en-2-one **16** (0.5 mg) [35] and the 11,12,13-tri-*nor*-eremophilene **17** (3.8 mg) [37].

The overexpressed mutant Ov*Bcstc3* broth afforded the reported polyketide derivatives **2** (1.2 mg) and **4** (2.0 mg) and the known compounds **6** (3.4 mg), **7** (5.2 mg), **10** (1.5 mg), **11** (3.6 mg) [36,54], **15** (1.5 mg) [35], **17** (3.4 mg) and **18** (1.1 mg) [37]. The chemical structures were determined by a wide range of spectral analyses using mono- and bidimensional resonance experiments and they were confirmed by direct comparison of their spectroscopic constants with those of authentic samples.

Finally, analysis of the metabolomic profile of both transformants, the null mutant Δ*Bcstc3* and the overexpressed Ov*Bcstc3*, seem to indicate that the production of secondary metabolites was not affected by mutations in the *Bcstc3*. So, both transformants produced polyketide botcinins, as well as eremophilenol derivatives. Additionally, the Δ*Bcstc3* biosynthesized the keto derivative **16** and the 11,12,13-tri-*nor*-eremophilene **17**, while the Ov*Bcstc3* mutants produced the keto derivative **15** and the two 11,12,13-tri-*nor*-eremophilenes **17** and **18**, all of them previously reported (Figure 11) [35–37]. Unfortunately, no new metabolites were detected/produced by the overexpressed transformant.

3. Discussion

The annotation of the *B. cinerea* B05.10 genome showed six genes putatively encoding for sesquiterpene cyclases. Three members of this gene family have previously been characterized. *Bcstc1*/*Bcbot2* encodes for a pentalenene cyclase, which catalyzes the first step in the biosynthesis of the botrydial phytotoxin and other important derived sesquiterpenes, generating the precursor tricyclic alcohol presilphiperfolan-8β-ol [29,30]. The deletion of the *Bcsct5* gene in the ABA-overproducer strain ATCC58025 let us conclude that BcStc5/BcAba5 is the key enzyme responsible for the sesquiterpenoid abscisic acid biosynthesis [31], and the sesquiterpene cyclase 7 (BcStc7) catalyzes the cyclization of farnesyl diphosphate to eremophil-9-en-11-ols [35–37]. Finally, the *Bcstc2* gene is related to the cryptic metabolite botrycinereic acid synthesis [55]. Here, the role of another member of this family, the BcStc3 protein, in the biology of *B. cinerea* is unravelled.

3.1. Bcstc3 Encodes for a Terpene Synthase Family 2, C-Terminal Metal Binding Domain Protein

The *Bcstc3* gene encodes for a terpene synthase family 2, C-terminal metal binding domain protein (Pfam 19086), according to the BLAST search against the NCBI non-redundant protein database, the same protein family of the pentalenene cyclase BcStc1/BcBot2 [29,30], the BcStc5 protein involved in the farnesyl diphosphate conversion into 2*Z*-4*E*-α-ionylideneethane [31], and the yet-to-be characterized BcStc4. The two remaining genes of the *Bcstc* family, *Bcstc2* and *Bcstc7*, encode for trichodiene synthases (Pfam 06330). Both enzyme families are members of the class I terpene synthase (cd00868, EC 4.2.3.-) that share a common α-helical fold and use a trinuclear Mg^{2+} cluster to activate the substrate, isoprenoid pyrophosphate precursors, by ionization and cleavage of pyrophosphate, generating several carbocation intermediates conducting to the cyclization of the substrate [56–58]. Indeed, the features conserved across this enzyme class are two conserved motifs involved in the magnesium binding: two magnesium ions bound to the enzymes by a conserved aspartate-rich region (D(D/E)XX(D/E)) and the third one by an NSE/DTE ((N,D)D(L,I,V)X(S,T)XXXE motif) [56,57]. Both motifs are localized within the C-terminal or α-domain of the proteins, as in the BcStc3 sequence. The C-terminal region of the BcStc3 showed a higher conservation score containing the two canonical motifs involved in catalysis in class I terpene cyclase. The aspartate-rich motif was identified at position 177, for the first aspartate residue, and at residue 307, for the N of the NSE/DTE motif (Figure 1). Two other motifs involved in catalysis were also identified in the BcStc3 sequence: the conserved effector triad (R264-D267-I268 residues) that also coordinate the ppi, aiding in substrate recognition and is associated with the initiation of the cyclization reaction [47,56,57], and the conserved RY pair (R334-Y335 residues) (Figure 1) that is involved in the PPi recognition through hydrogen bonds [47,59]. The arginine residue in the RY pair of BcStc1/BcBot2 (R373) plays a significant role after the formation of the caryophyllenyl cation [59]. Two of the three residues involved in the selectivity of BcStc1/BcBot2 (W94, F99 and N325 residues) [47] were identified in the sequence of BcStc3 (F174 and

 doi:10.20944/preprints202403.1652.v1

N392 residues, Figure 1), probably also related to the selectivity of the enzyme. In addition, the substrate binding to the active site of BcStc1/BcBot2 induced conformational changes of these motifs and the H-α1 loop, too [47]. It has been shown that this loop moves and shields the active site upon the formation of an Mg2+3-PPi complex of BcStc1/BcBot2 and the sesquiterpene cyclases Cop3, Cop4, and Cop6 from the basidiomycete *Coprinus cinereus*, modulating the selectivity of these enzymes [50]. The loop was also identified in the 3D model of BcStc3, as the conserved asparagine residue (N329 residue) at the C-terminus (Figure 2) that interacts with an aspartic residue of the NSE/DTE motif to place the H-α1 loop at the active [50].

3.2. BcStc3 is a Well Conserved Protein in Botrytis Genus

The BcStc3 protein is a well-conserved protein in the *Botrytis* genus, especially in species that infect monocots Lliaceae (*B. tulipae*, *B. elliptica*), Amaryllidaceae (*B. sinoalli*, *Botryotinia globosa*, *B. byssoidea*, *Botryotinia narcissicola*, and *B. galanthina*), Hyancinthaceae (*B. hyacinthi*), and Asphodelaceae (*B. deweyae*) (Figure 3). The orthologous proteins of Bcstc3 in *B. elliptica*, *B. hyacinthi*, *B. galanthina*, and *B. narcissicola* had been previously identified [60], but this is the first time that homologous to this sesquiterpene cyclase are identified in *B. sinoallii*, *B. tulipae*, *B. deweyae*, *B. byssoidea* and *Botryotinia globosa* (Figure 3, Supplementary Figure S1). The phylogenetic tree of these proteins closely resembled that previously described for *Botrytis* genes [61,62]. BcSct3 grouped apart in clade I, while the rest formed clade II, with the proteins of *B. deweyae*, *B. elliptica*, and *B. sinoalli* forming a separate subclade according to [61]. Unexpectedly, the BcStc3-homologous protein of *B. byssoidea* grouped apart (Figure 3), despite this species is phylogenetically close to *Botryotinia narcissicola*, *B. tulipae*, and *Botryotinia globosa* [61]. The sequence alignment confirmed that the aspartic-rich domain DDMWE in the XP_038737186.1 protein is not conserved (Supplementary Figure S1).

3.3. BcStc3 is a Well Conserved Protein in Kingdom Fungi

BcSTc3 protein is also a well-conserved protein among the kingdom Fungi. Homologous proteins to BcStc3 were identified in 124 fungal species, excluding the *Botrytis* genus. Seven of these proteins were found in three species of the Strophariaceae family and the remaining 153 proteins were distributed along 121 species of different Ascomycota, mainly of the Eurotiomycetes, Dothideomycetes, and Sordariomycetes classes. The ratio of Bcstc3-homologous proteins per organism was slightly higher in Basidiomycota than in Ascomycota. This difference between phyla has been previously described for terpene synthases and may be related to tandem duplication of the gene clusters in Basidiomycota [46,63,64]. Of the 160 BcStc3 homologous proteins, only one has been previously characterized and crystalized, the terpene cyclase AaTPS of *Alternaria alternata* [65]. AaTPS was characterized as a bifunctional enzyme using the same active site to catalyze terpene cyclization, and aromatic prenylation reactions favored the last ones under alkaline conditions [65]. The prenyltransferase activity might regulate isoprenoid diphosphate concentrations, avoiding toxic levels in the cell [65]. The study of this enzyme allowed to conclude that the bifunctional activity is well conserved among terpene cyclase family proteins and, therefore, it should be kept in mind the possibility that the BcStc3 protein may also function as an aromatic prenyltransferase in a pH-dependent manner.

The phylogenetic tree generated from the alignment of the first 55 sequences retrieved from the BlastP search using the BcStc3 sequence as query grouped BcStc3 with its homologous of *Rutstroemia* sp, other species of Helotiales order, as *B. cinerea*. This fungus is the causal agent of bleach blonde syndrome on cheatgrass that secretes diverse phytotoxic secondary metabolites involved in pathogenesis [66]. Surprisingly, these two proteins formed a subclade with the homologous protein of *Pycnora preastabilis*, a lichen fungus that affects mainly conifer trees. This fungus belongs to the recently established class Candelariomycetes and is characterized by a drastic reduction of the genome size and the number of secondary metabolite biosynthetic gene clusters [67,68]. Moreover, these three proteins clustered with numerous lichenised Ascomycota of the Lecanoromycete and Xylobotryomycete classes and fungi not phylogenetically related as the little brown mushroom

 doi:10.20944/preprints202403.1652.v1

Galerina marginata or polymorphic black yeast-like fungi, all of them producers of diverse classes of secondary metabolites, some of them with clinical applications [66,69,70].

3.4. Deletion of the Gene Encoding Sesquiterpene Cyclase 3 (Bcstc3).

This study focused on the deletion of the gene encoding sesquiterpene cyclase 3 (*Bcstc*3) and the generation of overexpressed *Bcstc*3 mutants in the *B. cinerea* UCA992 strain. We replaced the original gene ORF of *Bcstc*3 (Bcin13g05830) with an ORF conferring resistance to hygromycin in the wild-type strain. Following transformation and selective culturing, DNA extraction and conventional PCR confirmed homologous integration of the replacement fragment at the Bcstc3-5′ and -3′ regions, respectively identified by primer pairs *Bcstc*3-hi5F/*TrpC*-T (amplicon size: 1028 bp) and *Bcstc*3-hi3R/*TrpC*-P2 (amplicon size: 720 bp). The absence of *Bcstc*3 alleles in the mutants, demonstrating homokaryotic profiles devoid of parental nuclei containing the *Bcstc*3 gene, was validated using primers Bcstc3-WT-F/WT-R (absence of amplicon size: 520 bp) (Supplementary Table S1).

Additionally, overexpressed mutants (Ov*Bcstc3*) were created by introducing an extra copy of the *Bcstc*3 gene under the *actA* gene promoter and the *trpC* terminator (TtrpC) from *Aspergillus nidulans* into the *Bcnia*D gene locus, coding for nitrate reductase, in the wild-type strain, alongside a nourseothricin resistance cassette. The homologous integration at BcniaD-5′ and -3′ was confirmed using primer pairs BcniaD-hi5F/PactA-stc3-R (amplicon size: 4243 bp) and BcniaD-hi3R/PactA-amp-F (amplicon size 2174 bp), with the presence of *BcniaD* alleles in mutants corroborated by BcniaD-WT-F/WT-R primers (absence of amplicon size WT – 780 bp) (Supplementary Table 1).

3.5. Bcstc3 is Differentially Expressed during Fungal Development and Pathogenesis

The *Bcstc3* gene is not only expressed in non-germinated conidia but also up-regulated during fungal vegetative growth and during plant-host interaction up to 7 and 16 times compared to the expression level in no-germinated conidia (Figure 5). These results suggest a significant role of BcStc3 in the biology of *B. cinerea*. Actually, *Bcstc3*, along with the *Bcsct1* and *Bcstc2* genes, is one of the most induced genes *in planta*, and with *Bcstc4*, in axenic culture (Figure 5). This expression pattern, however, differs in some aspects from that in the B05.10 strain (Supplementary Figure S2). Overall, the family gene expression is higher in the B05.10 strain than in the UCA922, as it has been reported previously in different culture conditions [35,54]. Although, in ungerminated conidia of both strains, the *Bcsct5* mRNA was the most abundant, the least expressed genes were *Bcstc2* and *Bcstc1* in the UCA922 and B05.10 strains, respectively (Figure 5 and Supplementary Figure S2). On the other hand, during vegetative growth and *in planta*, the *Bcstc7* gene did not change its basal expression level in the UCA922 strain compared to ungerminated conidia, but this gene was the most overexpressed of the gene family in the B05.10 strain in axenic culture (more than 2000 times respect the expression level in ungerminated conidia) and the second one (more than 600 times) after *Bcstc1* (770-fold increase), *in planta* (Supplementary Figure S2).

Furthermore, the expression pattern is differentially regulated in a fungal strain-dependent manner and points to a functional specialization through differential expression patterns. Variations between strains were also observed in the gene family expression when the B05.10 and UCA922 strains were grown in sublethal levels of copper sulphate [54]. The generation of two new strains, the null *Bcstc3* mutant and the overexpressed-*Bcstc3* strain, allowed us to study the putative co-regulation of the *Bcstc* gene family in *B. cinerea* (Figure 6). In ungerminated conidia, the deletion of the *Bcstc3* gene caused the down-regulation of *Bcsct5*, but the contrary effect was observed when the *Bcstc3* gene was overexpressed, suggesting a close co-regulation of *Bcstc3* and *Bcstc5* genes (Figure 6). *Bcstc1*, *Bcstc2*, *Bcstc4* and *Bcstc7*, to a greater or lesser extent, were upregulated in ungerminated conidia of both transformants compared to the wild type (Figure 6). These findings suggest that the relative *Bcstc3* mRNA abundance affects the expression of the other *Bcstc* genes and point to the relevance of this gene family in conidial morphogenesis and/or viability. During vegetative growth, *Bcsct4*, *Bcstc5* and *Bcstc7* were up-regulated in both strains, and the *Bcstc1* level almost did not change compared to the basal expression in non-germinated conidia of each strain (Figure 6).

 doi:10.20944/preprints202403.1652.v1

3.6. BcStc3 is Involved in Fungal Development and Tolerance to Osmotic and Oxidative Stress

The putative role of the BcStc3 protein in the biology of *Botrytis* was ruled out by studying the fungal phenotypic changes due to the deletion or the constitutive expression of the *Bcstc3* gene in the Δ*Bcstc3* and Ov*Bcstc3* strains, respectively. The growth rate of both strains was reduced by 14% compared to the wild type on solid medium (Figure 7). However, the biomass of the Ov*Bcstc3* strain decreased by 21% when cultured on a liquid medium, while the mutant strain grew as the wild type (Figure 7). Probably, the secondary metabolite/s related to the BcStc3 enzymatic activity could affect the fungal ability to expand on a solid substrate, resulting in a reduction in growth rate in a solid medium. On the other hand, the putative terpenoid deficiency may be compensated by activating alternative metabolic pathways that enable growth and development in a liquid environment. In fact, we found that the deletion or the constitutive expression of the *Bcstc3* gene changed differentially the expression pattern of the rest of the *Bcstc* family genes during axenic culture, especially of *Bcstc2* (Figure 6). The role of *Bcstc7* and *Bcstc1*/*Bcbot2* in mycelial development has already been ruled out [30,35], but it yet to be established whether *Bcstc2*, *Bcstc4* and *Bcstc5* are involved in the fungal growth. Recently, it has been shown that the terpene cyclase-like 2 CcPtc1 of the necrotrophic phytopathogenic fungus *Cytospora chrysosperma* plays a relevant role in the development avoiding the accumulation of trehalose 6-phosphate that has a cytotoxic effect [71]. The specific role of Bcstc3 in vegetative growth of *B. cinerea* remains to be elucidated.

A strong correlation has been identified between the regulation of secondary metabolism and stress triggers and the involvement of the secondary metabolites in environmental adaptation and stress tolerance in filamentous fungi [72,73]. The profile of secondary metabolites produced and the regulatory cell components involved in each stress response vary depending on the type of stress [74,75]. Thus, the putative role of *Bcstc3* to overwhelm stress conditions was investigated by studying the effect of sorbitol and hydrogen peroxide on mycelium development when the protein was lacking or overproduced. The osmotic agent sorbitol caused a 15% reduction of the growth rate of the wild-type strain, but lack or overproduction of the BcStc3 protein slightly reduced or increased twice the sensitivity to this agent, respectively (Figure 7). We hypothesize that the secondary metabolites generated as end-products of the pathway in which Bcstc3 is involved may affect the ability of *B. cinerea* to respond effectively to osmotic stress conditions. Moreover, the reduced biomass in the liquid culture of the Ov*Bcstc3* strain compared to the Δ*Bcstc3* mutant and the wild type may be related to the differential tolerance to osmotic stress of the fungal strains (Figure 7). The overproduction of BcStc3 caused an increase in osmotic sensitivity that triggered a reduction of fungal biomass when the Ov*Bcstc3* strain was cultured in a liquid medium. On the contrary, the lack of *Bcstc3* increased tolerance to osmotic stress enough that the mycelial of the mutant strain development was not affected (Figure 7).

It has been extensively demonstrated that the induction of secondary metabolism is associated with oxidative stress protecting fungi from ROS damage [72,76]. Lycopene, lutein, perillic acid and eremanthin are examples of terpenes that act as direct antioxidants through free radical scavenging mechanisms, although these secondary metabolites may also act as indirect antioxidants by enhancing the antioxidant status (enzymatic and non-enzymatic) [77,78].

Therefore, BcStc3 is not related to ROS production and, probably, its absence activates alternative metabolic pathways or the overexpression of other antioxidant proteins in response to external hydrogen peroxide that enables scavenging the excess of the oxidant. The enhanced BcStc3 production may cause the accumulation of the secondary metabolites related to the enzymatic activity of the protein that triggers the production of ROS or alternative metabolic pathways that alter the redox balance within the cell. The additional stress caused by the overproduction of these compounds could also overload the antioxidant defence systems of the cell, resulting in an accumulation of reactive oxygen species. In *Aspergillus flavus*, oxidative stress upregulates the production of aflatoxins and the terpenoid kojic acid, along with the expression of monooxygenase genes [79,80]. Kojic acid binds free Fe cations preventing non-enzymatic ROS formation or directly reacts with ROS, reducing oxidants in the cell [80]. However, the overproduction of kojic acid causes iron deficiencies that may affect the regulation of siderophore biosynthetic genes and other signalling

 doi:10.20944/preprints202403.1652.v1

pathways [80]. In the basidiomycete *Ganoderma lucidum*, the decreased production of the triterpenoid ganoderic acid was accompanied by an increase in fungal resistance to oxidative stress (increasing intracellular ROS levels and inhibiting the enzymatic activity of the antioxidant systems) [81]. Overall, although the specific role of BcStc3 in the fungal response to oxidative stress remains the subject of further studies, it seems that BcStc3 is not involved in ROS production but in regulating detoxification systems.

3.7. BcStc3 is Involved in Conidial Morphogenesis and Infection Cushions Production

Secondary metabolism gene clusters exhibit increasingly dynamic and differential expression during asexual growth, conidiation, and sexual development in filamentous fungi [82,83]. The BcStc3 protein does not seem to be related to the production of conidia since the deletion or overexpression of the Bcstc3 gene did not cause any change in the ability to produce these asexual reproductive structures (Figure 9). However, BcStc3 plays a role in conidial morphogenesis, as the size and possibly the composition/structure of the surface of conidia changed when the BcStc3 protein was overproduced (Figure 9). Additionally, the protein is also involved in conidial germination. Its deficiency resulted in a 50% reduction in the germination rate, while overproduction led to a 17% increase compared to the wild type.

The role of other members of the *Bcstc* gene family of *B. cinerea* in conidiation has also been studied with different results. The deletion of the *Bcstc7* gene encoding for a sesquiterpene cyclase abolished the (+)-4-*epi*-eremophil-9-en-11-ols biosynthesis [35]. The role of these secondary metabolites in conidiation had been confirmed as the external addition of eremophilenols increased the formation of conidiophores [35]. Nevertheless, the deficiency of the *Bcbot2* protein involved in the botrydial biosynthesis did not affect conidial morphogenesis [30]. Finally, the deletion of the *Bcstc5*/*Bcaba5* gene did not induce any change in conidiation of the ABA-overproducing strain ATCC58025, which is known to be deficient in conidia and sclerotia formation [84].

The relationship between terpene biosynthesis and conidiation has been shown in other filamentous fungi. The *Ccptc* gene deletion, which encodes for a terpene cyclase in the phytopathogen fungus *Cytospora chrysosperma*, reduced the conidial production [71]. The Trt1 terpene cyclase of the opportunistic fungus *A. terreus* is involved in the biosynthesis of the mycotoxin terretonin, expressed in the conidia and activated during the germinating stage [85]. In this work, we studied the relative expression levels of the *Bcstc* gene family in conidia of the Δ*Bcstc3* and the Ov*Bcstc3* strains compared to those in the wild-type strain (Figure 6). The deletion or overexpression of *Bcstc3* led to differential changes in the expression of the remaining genes within the family. The most upregulated gene in the mutant strain was *Bcstc7* (Figure 7). *Bcstc5* showed the highest upregulation in the Ov*Bcstc3* strain but was repressed in the Δ*Bcstc3* strain (Figure 9). These different expression patterns of the *Bcstc* genes likely contribute to the variations observed in the germination rate, conidial size, and aggregation between both transformants (Figure 9). Additionally, terpenes can influence conidial morphogenesis and germination, interacting with specific receptors and cellular signaling pathways in filamentous fungi. Numerous transcriptional factors in *B. cinerea* involved in the regulation of the secondary metabolism also control conidiation and terpene production. The transcriptional factor BcReg1 and the regulator of the abscisic acid biosynthesis BcLae1 are two examples of factors upregulating conidial morphogenesis and biosynthesis of the sesquiterpene botrydial and the polyketide botcinic acid [86,87]. On the contrary, the BcVel1 and BcLTF1 factors differentially regulate the *Bcstc* gen family and repressed conidiation [88,89]. Finally, recently it has been described the role of the polyketide synthase PKS15 of the entomopathogenic fungus *Beauveria bassiana* in the cell wall formation. The pks15 mutation caused an alteration of mannan and glucan organization in the wall, generating more elongated conidia than the wild type with smoother surfaces [90]. The enzyme and its metabolite may act in cellular signaling, and it may also be possible that the PKS15 metabolite could directly be a spore wall component.

The infection cushions are specialized structures produced by certain pathogenic fungi formed by the aggregation of fungal hyphae and specialized cells at the site of infection [91]. The infection cushions enable the fungus to efficiently infect the plant by promoting the penetration and

 doi:10.20944/preprints202403.1652.v1

colonization of the host tissues, playing a crucial role in the pathogenicity and spread of fungal diseases in plants [92]. They serve as physical barriers that shield the fungal hyphae from the damaging effects of ROS produced by the host plant, displaying mechanisms such as the upregulation of antioxidant enzymes or the synthesis of protective metabolites [52]. We found that the overexpression of the *Bcstc3* gene resulted in a twofold increase in hydrogen peroxide production compared to both the wild-type and the mutant strains, which exhibited similar behavior to each other (Figure 10), and in a reduced tolerance to oxidative stress (Figure 7). Although the *Bcstc1*/*Bcbot2* and *Bcboa6* genes encoding for the core enzymes of the BOT and BOA biosynthetic gene clusters, respectively, have been ruled out as players in the development of infection cushions [93]. Choquer et al. (2021) have shown that both clusters are upregulated in these infective structures [28]. However, in that study, the expression of the *Bcstc3* gene was not detected [52]. Altogether, these results suggest that the increased infection cushion production by the Ov*Bcstc3* strain is more likely related to enhance ROS generation than a direct role of the protein.

3.8. BcStc3 in Involved in Virulence

Surprisingly, the *ΔBcstc3* strain exhibited a higher infection efficiency than the wild type in grape, tomato fruits, in gerbera petals and tobacco leaves (Figure 8). The *Bcstc3* overexpression restored infectivity to wild strain levels in grapefruits and tobacco leaves infection but caused a slight decrease in the disease index in tomato fruits compared to that of the UCA922 strain (Figure 8). *In planta*, the *Bcstc3* deletion induced significant changes in the expression pattern of the remaining *Bcstc* genes, particularly the upregulation of *Bcstc1*/*Bcbot2*, which displayed a 40-fold increase in relative expression compared to the wild-type strain (Figure 6). BcSct1/BcBot2 is involved in the synthesis of botrydial, a sesquiterpene that triggers the hypersensitive response on plant tissue, inducing accumulation of ROS and phenolic compounds and causing chlorosis and cell collapse [94]. The overexpression of the *Bcstc1*/*Bcbot2* gene during infection of tobacco leaves by the Δ*Bcstc3* transformant may be related to the increased production of ROS in the host interaction and the enhanced virulence of the Δ*Bcstc3* strain. Similarly, the null mutant of the *bcpks13* encoding for a polyketide synthase involved in the melanin synthesis caused larger lesions and accumulated ROS more rapidly and abundantly than the wild type at the infection site [95]. The mutant strain did not show any advantage in the expression of ROS synthesis genes compared with the wild type, indicating that infection by the mutants could induce much stronger plant responses compared with the wild-type strain [95]. The lack of the BcStc3 protein and the BcStc1/BcBot2 overproduction may modify the oxidative balance at the infection site, increasing the fungal capability to penetrate and invade host plant tissues.

During the Δ*Bcstc3*-tobacco leaves interaction, the *Bcstc7* gene was also upregulated, 10-fold compared to its expression level in the wild-type strain (Figure 6). This structural similarity between capsidiol and eremophilenols has suggested that the fungal secondary metabolites may module the plant defense response to facilitate the attack of the plan tissue [35,36]. The upregulation of *Bcsct7* in the Δ*Bcstc3* strain *in planta* may also be involved in the increased virulence of this strain. Probably, the overexpression of *Bcstc1*/*Bcbot2* in the *Bcstc3* mutant strain might also be accompanied by the upregulation of the BOA biosynthetic cluster affecting the virulence of this transformant, although it should be confirmed experimentally. BcLae1, a methyltransferase involved in the ABA biosynthesis control, is a positive regulator of the BOT and BOA clusters but represses the *Bcstc3*, *Bcstc4* and *Bcstc5* expression [86,88]. Moreover, *Bcbot2*, *Bcstc3* and *Bcstc4* are not related to a light response but are down-regulated by the action of BcLtf1, a modulator of the transcriptional responses to light, while *Bcstc5* is upregulated [89]. It cannot be ruled out that the alterations of the pathway in which BcStc3 participates might cause the biosynthesis of other secondary metabolites that could act as effectors, increasing the infective capacity of the fungus and/or modulating the plant defense response.

4. Materials and Methods

4.1. Bioinformatic Analysis

 doi:10.20944/preprints202403.1652.v1

The BcStc3 sequence was used as a query to perform a BlastP search against the non-redundant protein sequence database at the National Centre for Biotechnology Information (NCBI) [43]. Homologous proteins were selected from the resulting list following the criteria: percent identity (>30%), coverage (>70%), and the bit-score (>50) [51]. Sequence identities were calculated by the Sequence Identity And Similarity (SIAS) module from [http://imed.med.ucm.es/Tools/sias.html] [96]. Phylogenetic analyses were performed by the neighbor-joining method with 1000 bootstrap replicates using the Mega X software (Version 11) [97]. The predicted BcStc3 3-D model was obtained from the alphafold tool (https://alphafold.ebi.ac.uk/) [48,98], using the default parameters. The resulting protein structure was then visualized with PyMOL Molecular Graphics System (Version 1.8, Schrödinger, LLC).

4.2. Organisms, Media and Culture Conditions

The *Bcstc3* knock-out mutant and the Ov*Bcstc3* strain were generated in this work from the parental *B. cinerea* strain UCA992, obtained from Domecq vineyard (Jerez de la Frontera, Cádiz, Spain) and deposited in the Mycological Herbarium Collection of the University of Cádiz. All fungal strains were routinely grown in YGG medium (2% glucose, 0.5% yeast extract, 0.3% Gamborg's B5 medium (Duchefa Biochemie), and 1.5% agar, when needed) at 20°C for three days. Tomato agar plates (25% homogenized tomato fruits (w/v), 1.5% agar, pH 5.5) were used for conidia production. Potato dextrose agar (PDA) (Sigma-Aldrich) medium (1/4) was used to estimate the infection cushion production. The conidial stock suspensions were maintained in 10% glycerol at -80°C. For DNA extraction from mycelium, fungal strains were incubated in Petri dishes containing completed medium (CM) (10 g glucose, 2 g casein peptone, 1 g casamino acids, 1 g yeast extract, 50 mL salt solution, 1 mL vitamin solution (0.5 g biotin, 50 g nicotinamide, 16 g *p*-aminobenzoic acid and 20 g pyridoxine hydrochloride per liter) and 2 mL microelement solution (1 g $FeSO_4 \cdot 7H_2O$, 0.15 g $CuSO_4 \cdot 5H_2O$, 1.61 g $ZnSO_4 \cdot 7H_2O$, 0.1 g $MnSO_4 \cdot H_2O$, 0.1 g $(NH_4)_6Mo_7O_{24} \cdot 4H_2O$, per liter), per liter, pH 5.0) overlaid with cellophane for 3 to 4 days at 20°C.

For the *S. cerevisiae* strain FY834 [35,99] transformation, plates of SD-uracil medium (D-glucose 20 g, Difco® yeast nitrogen base without amino acids 6.7 g, Clontech –Ura DO supplement 0.77 g, agar 16 g, per liter, pH 5.8) were used, and they were incubate for 3 or 4 days at 30°C.

N. tabacum var. Havana plants were maintained in a growth chamber at 22°C, 70% humidity under a light/dark cycle of 14 h light/10 h dark. *Gerbera jamesonii*, grapes and tomato fruits were purchased from local groceries.

4.3. Standard Molecular Methods for Gene Inactivation and Overexpression

Fungal genomic DNA was isolated following the protocol of Mansfield (1985) [100]. Bacterial plasmids were isolated using the GeneJET PCR Plasmid Purification Kit (Thermo Scientific). NanoDrop 2000c spectrophotometer (Thermo- Scientific) was used for checking purity and concentration of DNA samples. Phusion High-Fidelity DNA Polymerase (Thermo-Scientific) and Go-Taq DNA Polymerase (Promega) were used for conventional PCR. Agarose gel electrophoresis and restriction enzyme digestions were performed using standard procedures [101]. For sequence analysis, DNASTAR Lasergene package (DNASTAR, Inc.) programs were used. Oligonucleotides (Supplementary Table S1) were from Metabion International AG.

4.4. Generation of the ΔBcstc3 and OvBcstc3 Strains

For the generation of *Bcstc3* (Bcin13g05830) deletion mutants, two regions flanking the Bcstc3 ORF of 910 bp and 630 bp were amplified using primer pairs *Bcstc3*-5F/-5R and *Bcstc3*-3F/-3R, respectively (Supplementary Table S1). The two DNA fragments were assembled with a hygromycin resistance cassette obtained by PCR using plasmid pCSN44 as template and primer pair *Hph*-F/-R and with the *EcoR*I/*Xho*I-digested plasmid pRS426 [102,103] by yeast recombinational cloning using the strain *S. cerevisiae* FY834 [35,99]. The resulting *Bcstc3*-replacement fragment (3029 bp) was amplified with primer pair *Bcstc3*-5F and *Bcstc3*-3R and used to transform protoplasts of the *B. cinerea*

 doi:10.20944/preprints202403.1652.v1

UCA992 strain generated as described previously by Schumacher (2012). Transformants were selected by hygromycin resistance [102]. Homokaryotic mutant strains were generated using a single-spore isolation protocol as described by Gonzalez-Rodriguez et al. [99] and Schumacher [102] and confirmed by PCR amplification with the primer pairs *Bcstc3*-WT-F and *Bcstc3*-WT-R (Supplementary Table 1). To confirm the homologous integration of the replacement cassette at the *Bcstc3* locus, fungal DNA was isolated and amplified with the primer pairs *Bcstc3*-hi5F /*TrpC*-T and *TrpC*-P2/*Bcstc3*-hi3R to detect targeted integration at 5′ or 3′ ends, respectively (Supplementary Table S1).

For the generation of the *Bcstc*3-overexpressed strain (Ov*Bcstc*3), the ORF of *Bcstc*3 (1758 bp) was amplified using primers T*trpC-Bcstc*3-F and P*actA-Bcstc*3-R with DNA from the parental strain UCA992 serving as the template. The amplicon was then assembled with a fragment containing the *actA* promoter (P*actA*), obtained by PCR using primers P*actA*-amp-F and P*actA*-P*trpC*-R (Supplementary Table S1), and the plasmid pNDN-AGT [68] as the template, followed by digestion with *Spe*I and *Not*I enzymes of the same plasmid in yeast FY834 [35,99], resulting in the vector pNDN-*Bcstc*3-OVER. This resulting vector contains the ORF *Bcstc*3 gene under the control of the *actA* gene promoter and the *trpC* terminator (TtrpC) from *A. nidulans* [67], along with a nourseothricin resistance cassette (PtrpC::nat1), flanked by fragments of the *B. cinerea Bcnia*D gene, encoding nitrate reductase. Protoplasts of the UCA992 strain were transformed with the *Bcstc*3Ov-replacement fragment (6400 bp), obtained by PCR amplification using primer pair BcniaD-5F and BcniaD-3R (Supplementary Table S1) and vector pNDN-*Bcstc*3-OVER as template. Transformants were selected for nourseothricin resistance, and heterokaryons were generated. The targeted integration of the Bcstc3 expression cassette at the *Bcnia*D locus was checked by PCR with primer pairs BcniaD-hi5F/PactA-stc3-R and BcniaD-hi3R/PactA-amp-F, and heterokaryotic mutants were confirmed by PCR amplification with the primer pairs BcniaD-WT-F and BcniaD-WT-R (Supplementary Table S1).

4.5. Quantitative Assessment of Gene Expression via qRT-PCR

The fungal mycelium from *B. cinerea* UCA992 wt, Δ*Bcstc3*, Ov*Bcstc3* and *B. cinerea* B05.10 wt used for total RNA extraction was collected by filtration from 30 mL of YGG medium inoculated with 5 µL of 105 conidia/mL and incubated at 20°C for four days in darkness. To study *in planta* gene expression, detached leaves of *N. tabacum* var. Havana plants were inoculated with 5 µL droplets of a conidial suspension of 10^5 conidia/mL in TGGK solution (60 mM KH_2PO_4, 10 mM glycine, 0.01% Tween 20, 100 mM glucose) of *B. cinerea* UCA992 wt, Δ*Bcstc3*, Ov*Bcstc3* and *B. cinerea* B05.10 wt and incubated for 96 hours at 22°C in darkness with 70% humidity. The infected areas were cut and frozen at -80°C until use. Mycelia and infected plant tissues were homogenized with a drill, and total RNA was extracted using Trizol Reagent (Sigma-Aldrich, T 9424), following the manufacturer's instructions.

cDNA synthesis from 1 µg of total RNA was performed using iScript cDNA Synthesis Kit (Bio-Rad, USA) according to the manufacturer's instructions. qRT-PCR was carried out on an iCycler iQ system (Bio-Rad, USA) using the iQ SyBR Green Supermix (Bio-Rad, USA) and primers listed in Supplementary Table S1. The *actA* (Bcin16g02020) and *B-tub* (Bcin01g08040) genes of *B. cinerea*, encoding for actin and tubulin, respectively, were used as internal controls to normalize the cDNA samples. The relative amount of mRNA was calculated by the *ΔΔCt* method [104] for the mean of three independent determinations of the threshold cycle (Ct). The results were represented as mean values of $2^{(\Delta\Delta Ct \pm SD)}$ normalized to the expression of each gene in non-germinated conidia.

4.6. Phenotypic Characterization of Fungal Transformants

4.6.1. Vegetative Growth and Tolerance to Stress Agents

Petri dishes containing YGG-agar medium were inoculated with 10 µL droplets of a conidial suspension of 5 x 10^6 conidia/mL and incubated at 20°C to test for altered fungal growth. The colony radii were measured daily for four days, and the radial growth rate was calculated by plotting the colony radius over time, which fitted to a linear model (Pearson's correlation coefficient value ($r^2 \geq 0.98$)). Results are presented as the mean values of the growth rates in cm/day ± standard deviation

 doi:10.20944/preprints202403.1652.v1

of at least six independent experiments. To assess the sensitivity of fungal strains to stress conditions, the YGG-agar medium was supplemented with 1.4 M Sorbitol or 1.5 mM H_2O_2 for osmotic or oxidative stress, respectively. The relative growth inhibition rate was calculated as follows: Inhibition rate(%)=[1 -(T_4 – T_3)/(C_4 – C_3)]× 100, where T and C represent the radius of the colonies (cm) in treated and control plates, respectively, and 4 and 3 the days of incubation at 20°C [105].

In order to evaluate fungal biomass accumulation in liquid culture, 30 mL of YGG medium was inoculated with 10 µL of a conidial suspension of 5 x 10^6 conidia/mL and incubated at 20°C without shaking for four days. Mycelia were harvested by filtration, washed with sterile water, and dried for 1 hour at room temperature to obtain the fresh weight. The dry weight was estimated by incubating the mycelium at 50°C until a constant weight was achieved (dry weight). The experiment was conducted in triplicate, and the results are presented as the mean values of the biomass (g) ± standard deviation.

4.6.2. Conidial Production and Germination

Tomato agar plates (25% homogenized tomato fruits (w/v), 1.5% agar, pH 5.5) were inoculated with agar plugs containing young mycelium (0.5-cm YGG-agar cubes), incubated for three days at 20°C in dark conditions, and exposed for 16 h to near-UV light at a distance of 30–40 cm. After seven more days in darkness, conidia were collected as described by van der Vlugt-Bergmans et al. [101] and quantified using a hemocytometer under a bright-field microscope (Olympus BX-50). The results are presented as the mean values ± standard deviation of six individual experiments.

To assess the conidial germination rate, aliquots of 20 µL of a 10^5 conidia/mL suspension in YGG medium were placed on a sterile glass slide and incubated at 20°C in the dark and humidity conditions. After 6 hours, bright-field pictures of conidia were taken with an Olympus BX-50 microscope, and in each field examined, at least 100 conidia were counted. Conidia were considered germinated when the elongating germ tube was longer than the conidial longitudinal diameter. Conidial germination rate values are expressed as the percentage of germinated conidia to the total conidia counted.

To study conidial aggregation, the percentage of conidia clustered in groups of two or more was calculated from random bright-field pictures of 10000 conidia in YGG incubated on a sterile glass slide for 6 hours at 20°C in high humidity conditions. On the other hand, conidial aggregation was also estimated from the conidial sedimentation out of the suspension. The optical density of a 10^8 conidia/mL suspension in water was measured at 600 nm, and of the remained suspended conidia after 2 hours at room temperature. The optical density values were used to estimate the conidial concentration using a standard curve prepared from dilutions of a conidial suspension of known concentration. The conidial aggregation was calculated using the following equation: % aggregated conidia = 100 x ((initial conidia concentration- final conidia concentration)/initial conidia concentration).

4.6.3. Virulence Assays

Detached tobacco leaves, gerbera petals, and tomatoes and grapefruits were inoculated with 5 µL droplets containing 2500 conidia in TGGK solution (60 mM KH2PO4, 10 mM glycine, 0.01% Tween 20 and 100 mM glucose), incubated in the dark at 20°C under conditions of high humidity, and photographed every 24 hours. The diameter and length of the lesions on tobacco leaves and gerbera petals, respectively, were measured using ImageJ software [106], and the lesion growth rate was calculated and expressed in cm/day or mm/day, as indicated in Figure 8.

A semi quantitative scale with four grades according to the severity of disease symptoms was used to evaluate the virulence of the fungus in fruits. The results are presented as the percentage of fruits in each disease grade to the total number of infected fruits (>30). Disease scores from 0 to 4 were subsequently converted to a percentage fruit disease index (%DI) as follows: [∑(disease rank × number of fruits)/(highest disease rank × total number of fruits)] ×100.

4.6.4. Reactive Oxygen Species and Infection Cushions Production

 doi:10.20944/preprints202403.1652.v1

Quantitative determination of H_2O_2 was performed incubating 24 mg of fresh mycelium with 1 mL of DAB solution for 5 hours at room temperature. The mycelium was harvested, and the optical density of the supernatant was measured at 471 nm. The absorbance values were compared with a standard curve prepared with known peroxide concentrations. The results were presented as ng of H_2O_2/mg of mycelium.

In vivo ROS was analyzed in tobacco leaves inoculated with 5 µL droplets of a 5×10^5 conidia/mL conidial suspension in TGGK solution and incubated for 48 hours at 20°C. Leaf discs, including the infected area, were cut and vacuum infiltrated for 1 hour with 1 mg/mL of DAB solution, pH 3.7. Discs were boiled in ethanol for 10 minutes to eliminate chlorophyll and photographed. ROS production was measured by ImageJ software, and values were expressed as the percentage of brown pixels detected around the infection point.

The production of infection cushions was assessed following the semiquantitative method described by Sekulska-Nalewajko et al. in 2016 [107].

4.7. Statistical Analysis

Statistical Analysis was performed with the SPSS v 24 (IBM) software package. The normal distribution of data was analyzed with the Kolmogorov-Smirnov (N>50 samples) or Shapiro Wilks (N<50 samples) tests. Depending upon the results from normality tests, statistical significance was analyzed with the T-test or the Mann-Whitney test for comparison of normally distributed or nonparametric data, respectively. Statistical tests were significant if p-value < 0.05.

4.8. Metabolomic Characterization of the ΔBcstc3 and Overexpressed OvBcstc3 Mutant Strains

For the metabolomic characterization, the fungal strains were grown on malt agar medium (20 g/L D-glucose, 20 g/L malt extract, 1 g/L peptone, 20 g/L agar, pH 6.5–7) at 25°C to produce mycelium plugs (0.8 mm) that were further used to inoculate medium for metabolite production. All studied strains were fermented in 40 Roux culture bottles (1000 mL), each containing 150 mL of modified Czapek-Dox medium (50 g glucose, 1 g yeast extract, 1 g K_2HPO_4, 2.5 g $NaNO_3$, 0.5 g $MgSO_4 \cdot 7H2O$, 0.01 g $FeSO_4 \cdot 7H_2O$, 0.005 g $CuSO_4 \cdot 5H_2O$, pH 6.5-7, 1L of water). Bottles were inoculated with six mycelium plugs per bottle and incubated for 27 days at 25°C on surface culture under day-light.

Then 6 L of culture medium from each of the mutant strains were filtered under vacuum to remove mycelium, and the filtrates were saturated with NaCl and subjected to liquid−liquid extraction with ethyl acetate (EtOAc × 3) and dried over with anhydrous sodium sulphate. After filtration, solvents were evaporated at reduced pressure to yield the crude extracts as yellow oils, 173 mg from (Δ*Bcstc3*) and 153 mg from (Ov*Bcstc3*). For metabolites isolation and characterization, the crude extracts were initially fractionated by column chromatography on silica gel, with a mixture of ethyl acetate/hexane containing increasing percentages (10−100%) of ethyl acetate. Different fractions were further purified by HPLC with a mixture of acetone, ethyl acetate and hexane. The metabolites purified were subjected to extensive spectroscopic analysis by ^{1}H-NMR and ^{13}C-NMR using 1D and 2D NMR, HRMS and IR techniques and their optical activity measured (α) for identification purposes.

5. Conclusions

This study has advanced our understanding of the sesquiterpene cyclase BcStc3's role in *B. cinerea*, shedding light on the molecular biology and pathogenicity of this phytopathogenic fungus. Through the generation and characterization of BcStc3-deficient and overexpressed mutant strains, we have unveiled the crucial involvement of BcStc3 in regulating the expression of genes within the sesquiterpene cyclase family and its impact on virulence, stress response, and secondary metabolite production.

Although the quest for new metabolites stemming from BcStc3 activity was not fulfilled, our findings significantly contribute to the phenotypic characterization of *B. cinerea*. We have identified notable differences in oxidative and osmotic stress tolerance, conidial morphology, and infection

cushion formation. These results emphasize BcStc3's importance not just in specific metabolite biosynthesis but also in the fungus's adaptation and survival under challenging environmental conditions and during host-pathogen interactions.

Furthermore, this work has illustrated the complexity of co-transcriptional regulation among *Bcstc* family genes, providing insights into the genetic networks that modulate *B. cinerea*'s pathogenicity. The detailed examination of interactions between BcStc3 and other secondary metabolism components lays a valuable foundation for future research aimed at unravelling the molecular mechanisms behind fungal pathogenicity and stress resistance.

In summary, our discoveries significantly expand the current understanding of *B. cinerea* biology and offer groundwork for developing disease control strategies by targeting key metabolic pathways. This study highlights the importance of comprehensive phenotypic characterization and gene expression analysis in revealing critical gene functions in complex biological contexts.

Supplementary Materials: The following supporting information can be downloaded at the website of this paper posted on Preprints.org. Figure S1: Alignment of BcStc3 and homologous protein sequences of other *Botrytis* species; Figure S2: Gene expression of the *Bstc* gene family in the *B. cinerea* B05.10 strain; Figure S3: Virulence assays; Table S1. Oligonucleotides used in this work. Table S2: List of the 160 species with a protein homologous to BcStc3 of *B. cinerea* identified by the Blastp tool.

Author Contributions: Conceptualization, C.Ga., N.B., C.G., and I.G.C.; methodology, V. C-R., I.S., J.A., J.C.; investigation, V. C-R., I. S., and C.G.; resources, J.A., J.C., and I.G.C.; writing—original draft preparation, V.C-R., N.B., I.S.,C.Ga.; writing—review and editing, C.Ga., J.C., C.G., J.A. and I.G.C.; supervision, J.A., N.B., C.G., C. Ga., and I.G.C.; project administration, I.G.C., J.C.; funding acquisition, J.C., J.A. and I.G.C. All authors have read and agreed to the published version of the manuscript."

Funding: This research was supported by a grant from PID-2021-1228990-B-C21 and -C22 funded by MCIN/AEI/10.13039/501100011033 and by "ERDF A way of making Europe".

Acknowledgments: Use of NMR facilities at the Servicio Centralizado de Ciencia y Tecnología (SCCYT) of the University of Cádiz is acknowledged. In addition, the authors would like to thank to the professors Pablo Martín Vasallo and Julio Tomás Ávila Marrero for providing the iCycler iQ system (Bio-Rad, USA) and its facilities to perform the Rt-PCR of this work.

Conflicts of Interest: The authors declare no conflicts of interest.

References

1. Minami, A.; Ozaki, T.; Liu, C.; Oikawa, H. Cyclopentane-forming di/sesterterpene synthases: widely distributed enzymes in bacteria, fungi, and plants. *Nat. Prod. Rep.* **2018**, *35*, 1330–1346, doi:10.1039/C8NP00026C.
2. Christianson, D.W. Unearthing the roots of the terpenome. *Curr. Opin. Chem. Biol.* **2008**, *12*, 141–150, doi:10.1016/j.cbpa.2007.12.008.
3. Awouafack, M.D.; Tane, P.; Kuete, V.; Eloff, J.N. Sesquiterpenes from the medicinal plants of Africa. In *Medicinal Plant Research in Africa*; Elsevier, 2013; pp. 33–103.
4. Tian, S.-H.; Zhang, C.; Zeng, K.-W.; Zhao, M.-B.; Jiang, Y.; Tu, P.-F. Sesquiterpenoids from *Artemisia vestita*. *Phytochemistry* **2018**, *147*, 194–202, doi:10.1016/j.phytochem.2018.01.004.
5. Zhang, C.; Wen, R.; Ma, X.-L.; Zeng, K.-W.; Xue, Y.; Zhang, P.-M.; Zhao, M.-B.; Jiang, Y.; Liu, G.-Q.; Tu, P.-F. Nitric Oxide Inhibitory Sesquiterpenoids and its dimers from *Artemisia freyniana*. *J. Nat. Prod.* **2018**, *81*, 866–878, doi:10.1021/acs.jnatprod.7b00947.
6. Xue, G.-M.; Li, X.-Q.; Chen, C.; Chen, K.; Wang, X.-B.; Gu, Y.-C.; Luo, J.-G.; Kong, L.-Y. Highly oxidized guaianolide sesquiterpenoids with potential anti-inflammatory activity from *Chrysanthemum indicum*. *J. Nat. Prod.* **2018**, *81*, 378–386, doi:10.1021/acs.jnatprod.7b00867.
7. Tan, Y.; Yang, B.; Lin, X.; Luo, X.; Pang, X.; Tang, L.; Liu, Y.; Li, X.; Zhou, X. Nitrobenzoyl sesquiterpenoids with cytotoxic activities from a marine-derived *Aspergillus ochraceus* fungus. *J. Nat. Prod.* **2018**, *81*, 92–97, doi:10.1021/acs.jnatprod.7b00698.
8. Kimani, N.M.; Matasyoh, J.C.; Kaiser, M.; Brun, R.; Schmidt, T.J. Antiprotozoal sesquiterpene lactones and other constituents from *Tarchonanthus camphoratus* and *Schkuhria pinnata*. *J. Nat. Prod.* **2018**, *81*, 124–130, doi:10.1021/acs.jnatprod.7b00747.
9. Wang, W.; Liu, Y.; Shi, C.; Pan, L.; Zhang, X.; Zou, J.-J. High energy density renewable fuels based on multicyclic sesquiterpene: Synthesis and performance. *Fuel* **2022**, *318*, 123665, doi:10.1016/j.fuel.2022.123665.

10. Cane, D.E. Enzymic formation of sesquiterpenes. *Chem. Rev.* **1990**, *90*, 1089–1103, doi:10.1021/cr00105a002.
11. Dolence, J.M.; Poulter, C.D. Electrophilic alkylations, isomerizations, and rearrangements. In *Comprehensive Natural Products Chemistry*; Elsevier, 1999; pp. 315–341.
12. Lesburg, C.A.; Caruthers, J.M.; Paschall, C.M.; Christianson, D.W. Managing and manipulating carbocations in biology: terpenoid cyclase structure and mechanism. *Curr. Opin. Struct. Biol.* **1998**, *8*, 695–703, doi:10.1016/S0959-440X(98)80088-2.
13. Christianson, D.W. Structural biology and chemistry of the terpenoid cyclases. *Chem. Rev.* **2006**, *106*, 3412–3442, doi:10.1021/cr050286w.
14. Davis, E.M.; Croteau, R. Cyclization enzymes in the biosynthesis of monoterpenes, sesquiterpenes, and diterpenes. In *Topics in Current Chemistry*; Springer, Berlin, Heidelberg, 2000; pp. 53–95.
15. Chizzola, R. Regular Monoterpenes and sesquiterpenes (essential oils). In *Natural Products*; Springer Berlin Heidelberg: Berlin, Heidelberg, 2013; pp. 2973–3008. ISBN 9783642221446.
16. Dai, Q.; Zhang, F.-L.; Feng, T. Sesquiterpenoids specially produced by fungi: structures, biological activities, chemical and biosynthesis (2015–2020). *J. Fungi* **2021**, *7*, 1026, doi:10.3390/jof7121026.
17. Shimada, A.; Kusano, M.; Takeuchi, S.; Fujioka, S.; Inokuchi, T.; Kimura, Y. Aspterric acid and 6-hydroxymellein, inhibitors of pollen development in *Arabidopsis thaliana*, produced by *Aspergillus terreus*. *Zeitschrift für Naturforsch. C* **2002**, *57*, 459–464, doi:10.1515/znc-2002-5-610.
18. White, G.A.; Taniguchi, E. The mode of action of helminthosporal. II. Effect on the permeability of plant cell membranes. *Can. J. Bot.* **1972**, *50*, 1415–1420, doi:10.1139/b72-170.
19. Xu, D.; Xue, M.; Shen, Z.; Jia, X.; Hou, X.; Lai, D.; Zhou, L. Phytotoxic secondary metabolites from fungi. *Toxins.* **2021**, *13*, 261, doi:10.3390/toxins13040261.
20. Dean, R.; van Kan, J.A.L.; Pretorius, Z.A.; Hammond-Kosack, K.E.; Di Pietro, A.; Spanu, P.D.; Rudd, J.J.; Dickman, M.; Kahmann, R.; Ellis, J.; et al. The top 10 fungal pathogens in molecular plant pathology. *Mol. Plant Pathol.* **2012**, *13*, 414–430, doi:10.1111/j.1364-3703.2011.00783.x.
21. Dalmais, B.; Schumacher, J.; Moraga, J.; Le Pêcheur, P.; Tudzynski, B.; Collado, I.G.; Viaud, M. The *Botrytis cinerea* phytotoxin botcinic acid requires two polyketide synthases for production and has a redundant role in virulence with botrydial. *Mol. Plant Pathol.* **2011**, *12*, 564–579, doi:10.1111/j.1364-3703.2010.00692.x.
22. Colmenares, A.J.; Aleu, J.; Durán-Patrón, R.; Collado, I.G.; Hernández-Galán, R. The putative role of botrydial and related metabolites in the infection mechanism of *Botrytis cinerea*. *J. Chem. Ecol.* **2002**, *28*, 997–1005, doi:10.1023/a:1015209817830.
23. Rossi, F.R.; Gárriz, A.; Marina, M.; Romero, F.M.; Gonzalez, M.E.; Collado, I.G.; Pieckenstain, F.L.; Rubén Rossi, F.; Gárriz, A.; Marina, M.; et al. The sesquiterpene botrydial produced by *Botrytis cinerea* induces the hypersensitive response on plant tissues and its action is modulated by salicylic acid and jasmonic acid signaling. *Mol. Plant-Microbe Interact.* **2011**, *24*, 888–896, doi:10.1094/MPMI-10-10-0248.
24. D'Ambrosio, J.M.; Gonorazky, G.; Sueldo, D.J.; Moraga, J.; Di Palma, A.A.; Lamattina, L.; Collado, I.G.; Laxalt, A.M. The sesquiterpene botrydial from *Botrytis cinerea* induces phosphatidic acid production in tomato cell suspensions. *Planta* **2018**, *247*, 1001–1009, doi:10.1007/s00425-018-2843-8.
25. Malmierca, M.G.; Izquierdo-Bueno, I.; Mccormick, S.P.; Cardoza, R.E.; Alexander, N.J.; Moraga, J.; Gomes, E. V.; Proctor, R.H.; Collado, I.G.; Monte, E.; et al. Botrydial and botcinins produced by *Botrytis cinerea* regulate the expression of *T richoderma arundinaceum* genes involved in trichothecene biosynthesis. *Mol. Plant Pathol.* **2016**, *17*, 1017–1031, doi:10.1111/mpp.12343.
26. Vignatti, P.; Gonzalez, M.E.; Jofré, E.C.; Bolívar-Anillo, H.J.; Moraga, J.; Viaud, M.; Collado, I.G.; Pieckenstain, F.L. Botrydial confers *Botrytis cinerea* the ability to antagonize soil and phyllospheric bacteria. *Fungal Biol.* **2020**, *124*, 54–64, doi:10.1016/j.funbio.2019.11.003.
27. da Silva Ripardo-Filho, H.; Coca Ruíz, V.; Suárez, I.; Moraga, J.; Aleu, J.; Collado, I.G. From genes to molecules, secondary metabolism in *Botrytis cinerea*: New insights into anamorphic and teleomorphic stages. *Plants* **2023**, *12*, 553, doi:10.3390/plants12030553.
28. Amselem, J.; Cuomo, C.A.; van Kan, J.A.L.L.; Viaud, M.; Benito, E.P.; Couloux, A.; Coutinho, P.M.; de Vries, R.P.; Dyer, P.S.; Fillinger, S.; et al. Genomic analysis of the necrotrophic fungal pathogens *Sclerotinia sclerotiorum* and *Botrytis cinerea*. *PLoS Genet.* **2011**, *7*, e1002230, doi:10.1371/journal.pgen.1002230.
29. Porquier, A.; Morgant, G.; Moraga, J.; Dalmais, B.; Luyten, I.; Simon, A.; Pradier, J.-M.; Amselem, J.; Collado, I.G.; Viaud, M. The botrydial biosynthetic gene cluster of *Botrytis cinerea* displays a bipartite genomic structure and is positively regulated by the putative Zn(II)2Cys6 transcription factor *BcBot6*. *Fungal Genet. Biol.* **2016**, *96*, 33–46, doi:10.1016/j.fgb.2016.10.003.
30. Pinedo, C.; Wang, C.M.; Pradier, J.M.; Dalmais, B.; Choquer, M.; Le Pêcheur, P.; Morgant, G.; Collado, I.G.; Cane, D.E.; Viaud, M. Sesquiterpene synthase from the botrydial biosynthetic gene cluster of the phytopathogen *Botrytis cinerea*. *ACS Chem. Biol.* **2008**, *3*, 791–801, doi:10.1021/CB800225V/SUPPL_FILE/CB800225V_SI_001.PDF.
31. Izquierdo-Bueno, I.; González-Rodríguez, V.E.; Simon, A.; Dalmais, B.; Pradier, J.; Le Pêcheur, P.; Mercier, A.; Walker, A.; Garrido, C.; Collado, I.G.; et al. Biosynthesis of abscisic acid in fungi: identification of a

sesquiterpene cyclase as the key enzyme in *Botrytis cinerea*. *Environ. Microbiol.* **2018**, *20*, 2469–2482, doi:10.1111/1462-2920.14258.

32. Otto, M.; Teixeira, P.G.; Vizcaino, M.I.; David, F.; Siewers, V. Integration of a multi-step heterologous pathway in *Saccharomyces cerevisiae* for the production of abscisic acid. *Microb. Cell Fact.* **2019**, *18*, 205, doi:10.1186/s12934-019-1257-z.
33. Takino, J.; Kozaki, T.; Ozaki, T.; Liu, C.; Minami, A.; Oikawa, H. Elucidation of biosynthetic pathway of a plant hormone abscisic acid in phytopathogenic fungi. *Biosci. Biotechnol. Biochem.* **2019**, *83*, 1642–1649, doi:10.1080/09168451.2019.1618700.
34. Takino, J.; Kozaki, T.; Sato, Y.; Liu, C.; Ozaki, T.; Minami, A.; Oikawa, H. Unveiling biosynthesis of the phytohormone abscisic acid in fungi: Unprecedented mechanism of core scaffold formation catalyzed by an unusual sesquiterpene synthase. *J. Am. Chem. Soc.* **2018**, *140*, 12392–12395, doi:10.1021/jacs.8b08925.
35. Suárez, I.; González-Rodríguez, V.E.; Viaud, M.; Garrido, C.; Collado, I.G. Identification of the sesquiterpene cyclase involved in the biosynthesis of (+)-4-*epi*-eremophil-9-en-11-ol derivatives isolated from *Botrytis cinerea*. *ACS Chem. Biol.* **2020**, *15*, 2775–2782, doi:10.1021/acschembio.0c00561.
36. Suárez, I.; da Silva Lima, G.; Conti, R.; Pinedo, C.; Moraga, J.; Barúa, J.; de Oliveira, A.L.L.; Aleu, J.; Durán-Patrón, R.; Macías-Sánchez, A.J.; et al. Structural and biosynthetic studies on eremophilenols related to the phytoalexin capsidiol, produced by *Botrytis cinerea*. *Phytochemistry* **2018**, *154*, 10–18, doi:10.1016/j.phytochem.2018.06.010.
37. Suárez, I.; Pinedo, C.; Aleu, J.; Durán-Patrón, R.; Macías-Sánchez, A.J.; Hernández-Galán, R.; Collado, I.G. The complemented mutant Δ*Bcstc7*, in the STC7 of *Botrytis cinerea* led to the characterization of 11,12,13-tri-*nor*-eremophilenols derivatives. *Phytochemistry* **2022**, *193*, 113003, doi:10.1016/j.phytochem.2021.113003.
38. Paysan-Lafosse, T.; Blum, M.; Chuguransky, S.; Grego, T.; Pinto, B.L.; Salazar, G.A.; Bileschi, M.L.; Bork, P.; Bridge, A.; Colwell, L.; et al. InterPro in 2022. *Nucleic Acids Res.* **2023**, *51*, D418–D427, doi:10.1093/nar/gkac993.
39. Marchler-Bauer, A.; Derbyshire, M.K.; Gonzales, N.R.; Lu, S.; Chitsaz, F.; Geer, L.Y.; Geer, R.C.; He, J.; Gwadz, M.; Hurwitz, D.I.; et al. CDD: NCBI's conserved domain database. *Nucleic Acids Res.* **2015**, *43*, D222–D226, doi:10.1093/nar/gku1221.
40. Lu, S.; Wang, J.; Chitsaz, F.; Derbyshire, M.K.; Geer, R.C.; Gonzales, N.R.; Gwadz, M.; Hurwitz, D.I.; Marchler, G.H.; Song, J.S.; et al. CDD/SPARCLE: the conserved domain database in 2020. *Nucleic Acids Res.* **2020**, *48*, D265–D268, doi:10.1093/nar/gkz991.
41. Marchler-Bauer, A.; Bo, Y.; Han, L.; He, J.; Lanczycki, C.J.; Lu, S.; Chitsaz, F.; Derbyshire, M.K.; Geer, R.C.; Gonzales, N.R.; et al. CDD/SPARCLE: functional classification of proteins via subfamily domain architectures. *Nucleic Acids Res.* **2017**, *45*, D200–D203, doi:10.1093/nar/gkz991.
42. Kanehisa, M.; Sato, Y.; Morishima, K. BlastKOALA and GhostKOALA: KEGG tools for functional characterization of genome and metagenome sequences. *J. Mol. Biol.* **2016**, *428*, 726–731, doi:10.1016/j.jmb.2015.11.006.
43. Camacho, C.; Coulouris, G.; Avagyan, V.; Ma, N.; Papadopoulos, J.; Bealer, K.; Madden, T.L. BLAST+: architecture and applications. *BMC Bioinformatics* **2009**, *10*, 421, doi:10.1186/1471-2105-10-421.
44. Chang, H.; Cheng, T.; Wang, A.H. -J. Structure, catalysis, and inhibition mechanism of prenyltransferase. *IUBMB Life* **2021**, *73*, 40–63, doi:10.1002/iub.2418.
45. Aaron, J.A.; Christianson, D.W. Trinuclear metal clusters in catalysis by terpenoid synthases. *Pure Appl. Chem.* **2010**, *82*, 1585–1597, doi:10.1351/PAC-CON-09-09-37.
46. Nosenko, T.; Zimmer, I.; Ghirardo, A.; Köllner, T.G.; Weber, B.; Polle, A.; Rosenkranz, M.; Schnitzler, J.-P. Predicting functions of putative fungal sesquiterpene synthase genes based on multiomics data analysis. *Fungal Genet. Biol.* **2023**, *165*, 103779, doi:10.1016/j.fgb.2023.103779.
47. Lou, T.; Li, A.; Xu, H.; Pan, J.; Xing, B.; Wu, R.; Dickschat, J.S.; Yang, D.; Ma, M. Structural insights into three sesquiterpene synthases for the biosynthesis of tricyclic sesquiterpenes and chemical space expansion by structure-based mutagenesis. *J. Am. Chem. Soc.* **2023**, doi:10.1021/jacs.3c00278.
48. Varadi, M.; Anyango, S.; Deshpande, M.; Nair, S.; Natassia, C.; Yordanova, G.; Yuan, D.; Stroe, O.; Wood, G.; Laydon, A.; et al. AlphaFold Protein Structure Database: massively expanding the structural coverage of protein-sequence space with high-accuracy models. *Nucleic Acids Res.* **2022**, *50*, D439–D444, doi:10.1093/nar/gkab1061.
49. Wendt, K.U.; Schulz, G.E. Isoprenoid biosynthesis: manifold chemistry catalyzed by similar enzymes. *Structure* **1998**, *6*, 127–133, doi:10.1016/S0969-2126(98)00015-X.
50. López-Gallego, F.; Wawrzyn, G.; Schmidt-Dannert, C. Selectivity of fungal sesquiterpene synthases: role of the active site's H-1α loop in catalysis. *Appl. Environ. Microbiol.* **2010**, *76*, 7723–7733, doi:10.1128/AEM.01811-10.
51. Pearson, W.R. An introduction to sequence similarity ("homology") searching. *Curr. Protoc. Bioinforma.* **2013**, *42*, doi:10.1002/0471250953.bi0301s42.

52. Choquer, M.; Rascle, C.; Gonçalves, I.R.; de Vallée, A.; Ribot, C.; Loisel, E.; Smilevski, P.; Ferria, J.; Savadogo, M.; Souibgui, E.; et al. The infection cushion of *Botrytis cinerea*: a fungal 'weapon' of plant-biomass destruction. *Environ. Microbiol.* **2021**, *23*, 2293–2314, doi:10.1111/1462-2920.15416.
53. Tani, H.; Koshino, H.; Sakuno, E.; Cutler, H.G.; Nakajima, H. Botcinins E and F and botcinolide from *Botrytis cinerea* and structural revision of botcinolides. *J. Nat. Prod.* **2006**, *69*, 722–725, doi:10.1021/np060071x.
54. Pinedo, C.; Moraga, J.; Barua, J.; González-Rodríguez, V.E.; Aleu, J.; Durán-Patrón, R.; Macías-Sánchez, A.J.; Hanson, J.R.; Viaud, M.; Hernández-Galán, R.; et al. Chemically induced cryptic sesquiterpenoids and expression of sesquiterpene cyclases in *Botrytis cinerea* revealed new sporogenic (+)-4-*epi*-eremophil-9-en-11-ols. *ACS Chem. Biol.* **2016**, *11*, 1391–1400, doi:10.1021/acschembio.5b00931.
55. Pinto, A.A.; Barúa, J.E.; Almeida, M.O.; Viaud, M.; Zorrilla, D.; Collado, I.G.; Macías-Sánchez, A.J.; Durán-Patrón, R. Structural and biosynthetic studies of botrycinereic acid, a new cryptic metabolite from the fungus *Botrytis cinerea*. *Bioorg. Chem.* **2022**, *127*, 105979, doi:10.1016/j.bioorg.2022.105979.
56. Whitehead, J.N.; Leferink, N.G.H.; Johannissen, L.O.; Hay, S.; Scrutton, N.S. Decoding catalysis by terpene synthases. *ACS Catal.* **2023**, *13*, 12774–12802, doi:10.1021/acscatal.3c03047.
57. T, R.; Sharma, D.; Lin, F.; Choong, Y.K.; Lim, C.; Jobichen, C.; Zhang, C. Structural understanding of fungal terpene synthases for the formation of linear or cyclic terpene products. *ACS Catal.* **2023**, *13*, 4949–4959, doi:10.1021/acscatal.2c05598.
58. González-Hernández, R.A.; Valdez-Cruz, N.A.; Macías-Rubalcava, M.L.; Trujillo-Roldán, M.A. Overview of fungal terpene synthases and their regulation. *World J. Microbiol. Biotechnol.* **2023**, *39*, 194, doi:10.1007/s11274-023-03635-y.
59. Nikolaiczyk, V.; Irwan, J.; Nguyen, T.; Fohrer, J.; Elbers, P.; Schrank, P.; Davari, M.D.; Kirschning, A. Rational reprogramming of the sesquiterpene synthase BcBot2 yields new terpenes with presilphiperfolane skeleton. *Catal. Sci. Technol.* **2023**, *13*, 233–244, doi:10.1039/D2CY01617F.
60. Valero-Jiménez, C.A.; Veloso, J.; Staats, M.; van Kan, J.A.L. Comparative genomics of plant pathogenic *Botrytis* species with distinct host specificity. *BMC Genomics* **2019**, *20*, 203, doi:10.1186/s12864-019-5580-x.
61. Valero-Jiménez, C.A.; Steentjes, M.B.F.; Slot, J.C.; Shi-Kunne, X.; Scholten, O.E.; van Kan, J.A.L. Dynamics in secondary metabolite gene clusters in otherwise highly syntenic and stable genomes in the fungal genus *Botrytis*. *Genome Biol. Evol.* **2020**, *12*, 2491–2507, doi:10.1093/gbe/evaa218.
62. Garfinkel, A.R. The History of *Botrytis* taxonomy, the rise of phylogenetics, and implications for species recognition. *Phytopathology* **2021**, *111*, 437–454, doi:10.1094/PHYTO-06-20-0211-IA.
63. Hage, H.; Couillaud, J.; Salamov, A.; Loussouarn-Yvon, M.; Durbesson, F.; Ormeño, E.; Grisel, S.; Duquesne, K.; Vincentelli, R.; Grigoriev, I.; et al. An HMM approach expands the landscape of sesquiterpene cyclases across the kingdom fungi. *Microb. Genomics* **2023**, *9*, doi:10.1099/mgen.0.000990.
64. Robey, M.T.; Caesar, L.K.; Drott, M.T.; Keller, N.P.; Kelleher, N.L. An interpreted atlas of biosynthetic gene clusters from 1,000 fungal genomes. *Proc. Natl. Acad. Sci.* **2021**, *118*, doi:10.1073/pnas.2020230118.
65. He, H.; Bian, G.; Herbst-Gervasoni, C.J.; Mori, T.; Shinsky, S.A.; Hou, A.; Mu, X.; Huang, M.; Cheng, S.; Deng, Z.; et al. Discovery of the cryptic function of terpene cyclases as aromatic prenyltransferases. *Nat. Commun.* **2020**, *11*, 3958, doi:10.1038/s41467-020-17642-2.
66. Masi, M.; Meyer, S.; Górecki, M.; Pescitelli, G.; Clement, S.; Cimmino, A.; Evidente, A. Phytotoxic activity of metabolites isolated from *Rutstroemia* sp.n., the causal agent of bleach blonde syndrome on cheatgrass (*Bromus tectorum*). *Molecules* **2018**, *23*, 1734, doi:10.3390/molecules23071734.
67. Díaz-Escandón, D.; Tagirdzhanova, G.; Vanderpool, D.; Allen, C.C.G.; Aptroot, A.; Češka, O.; Hawksworth, D.L.; Huereca, A.; Knudsen, K.; Kocourková, J.; et al. Genome-level analyses resolve an ancient lineage of symbiotic ascomycetes. *Curr. Biol.* **2022**, *32*, 5209-5218.e5, doi:10.1016/j.cub.2022.11.014.
68. Voglmayr, H.; Fournier, J.; Jaklitsch, W.M. Two new classes of Ascomycota : Xylobotryomycetes and Candelariomycetes. *Persoonia - Mol. Phylogeny Evol. Fungi* **2019**, *42*, 36–49, doi:10.3767/persoonia.2019.42.02.
69. Schafhauser, T.; Wibberg, D.; Binder, A.; Rückert, C.; Busche, T.; Wohlleben, W.; Kalinowski, J. Genome assembly and genetic traits of the pleuromutilin-producer *Clitopilus passeckerianus* DSM1602. *J. Fungi* **2022**, *8*, 862, doi:10.3390/jof8080862.
70. Tesei, D. Black fungi research: out-of-this-world implications. *Encyclopedia* **2022**, *2*, 212–229, doi:10.3390/encyclopedia2010013.
71. Yang, Y.; Yu, L.; Qiu, X.; Xiong, D.; Tian, C. A putative terpene cyclase gene (CcPtc1) is required for fungal development and virulence in *Cytospora chrysosperma*. *Front. Microbiol.* **2023**, *14*, doi:10.3389/fmicb.2023.1084828.
72. Montibus, M.; Pinson-Gadais, L.; Richard-Forget, F.; Barreau, C.; Ponts, N. Coupling of transcriptional response to oxidative stress and secondary metabolism regulation in filamentous fungi. *Crit. Rev. Microbiol.* **2015**, *41*, 295–308, doi:10.3109/1040841X.2013.829416.
73. Umar, A.; Darwish, D.B.E.; Albalwe, F.M. Fungal secondary metabolites and their role in stress management. In *Fungal Secondary Metabolites*; Elsevier, 2024; pp. 15–56.

74. Overy, D.; Correa, H.; Roullier, C.; Chi, W.-C.; Pang, K.-L.; Rateb, M.; Ebel, R.; Shang, Z.; Capon, R.; Bills, G.; et al. Does Osmotic stress affect natural product expression in fungi? *Mar. Drugs* **2017**, *15*, 254, doi:10.3390/md15080254.
75. Ochiai, N.; Tokai, T.; Nishiuchi, T.; Takahashi-Ando, N.; Fujimura, M.; Kimura, M. Involvement of the osmosensor histidine kinase and osmotic stress-activated protein kinases in the regulation of secondary metabolism in *Fusarium graminearum*. *Biochem. Biophys. Res. Commun.* **2007**, *363*, 639–644, doi:10.1016/j.bbrc.2007.09.027.
76. Hong, S.-Y.; Roze, L.; Linz, J. Oxidative stress-related transcription factors in the regulation of secondary metabolism. *Toxins (Basel).* **2013**, *5*, 683–702, doi:10.3390/toxins5040683.
77. Liu, T.-T.; Xiao, H.; Xiao, J.-H.; Zhong, J.-J. Impact of oxygen supply on production of terpenoids by microorganisms: State of the art. *Chinese J. Chem. Eng.* **2021**, *30*, 46–53, doi:10.1016/j.cjche.2020.12.006.
78. Gonzalez-Burgos, E.; Gomez-Serranillos, M.P. Terpene compounds in nature: A review of their potential antioxidant activity. *Curr. Med. Chem.* **2012**, *19*, 5319–5341, doi:10.2174/092986712803833335.
79. Fountain, J.; Scully, B.; Chen, Z.-Y.; Gold, S.; Glenn, A.; Abbas, H.; Lee, R.; Kemerait, R.; Guo, B. Effects of hydrogen peroxide on different toxigenic and atoxigenic isolates of *Aspergillus flavus*. *Toxins (Basel).* **2015**, *7*, 2985–2999, doi:10.3390/toxins7082985.
80. Fountain, J.C.; Bajaj, P.; Pandey, M.; Nayak, S.N.; Yang, L.; Kumar, V.; Jayale, A.S.; Chitikineni, A.; Zhuang, W.; Scully, B.T.; et al. Oxidative stress and carbon metabolism influence *Aspergillus flavus* transcriptome composition and secondary metabolite production. *Sci. Rep.* **2016**, *6*, 38747, doi:10.1038/srep38747.
81. Zhang, G.; Zhang, C.; Leng, D.; Yan, P.; Wang, Z.; Zhang, M.; Wu, Z. The non-canonical functions of telomerase reverse transcriptase gene GlTert on regulating fungal growth, oxidative stress, and ganoderic acid biosynthesis in *Ganoderma lucidum*. *Appl. Microbiol. Biotechnol.* **2021**, *105*, 7353–7365, doi:10.1007/s00253-021-11564-9.
82. Wang, Z.; Lopez-Giraldez, F.; Slot, J.; Yarden, O.; Trail, F.; Townsend, J.P. Secondary metabolism gene clusters exhibit increasingly dynamic and differential expression during asexual growth, conidiation, and sexual development in *Neurospora crassa*. *mSystems* **2022**, *7*, doi:10.1128/msystems.00232-22.
83. Wang, Y.; Wu, J.; Yan, J.; Guo, M.; Xu, L.; Hou, L.; Zou, Q. Comparative genome analysis of plant ascomycete fungal pathogens with different lifestyles reveals distinctive virulence strategies. *BMC Genomics* **2022**, *23*, 34, doi:10.1186/s12864-021-08165-1.
84. Izquierdo-Bueno, I.; González-Rodríguez, V.E.; Simon, A.; Dalmais, B.; Pradier, J.; Le Pêcheur, P.; Mercier, A.; Walker, A.; Garrido, C.; Collado, I.G.; et al. Biosynthesis of abscisic acid in fungi: identification of a sesquiterpene cyclase as the key enzyme in *Botrytis cinerea*. *Environ. Microbiol.* **2018**, *20*, 2469–2482, doi:10.1111/1462-2920.14258.
85. Shankar, J.; Tiwari, S.; Shishodia, S.K.; Gangwar, M.; Hoda, S.; Thakur, R.; Vijayaraghavan, P. Molecular insights into development and virulence determinants of *Aspergilli*: A proteomic perspective. *Front. Cell. Infect. Microbiol.* **2018**, *8*, doi:10.3389/fcimb.2018.00180.
86. Wei, Z.; Shu, D.; Sun, Q.; Chen, D.; Li, Z.; Luo, D.; Yang, J.; Tan, H. The BcLAE1 is involved in the regulation of ABA biosynthesis in *Botrytis cinerea* TB-31. *Front. Microbiol.* **2022**, *13*, doi:10.3389/fmicb.2022.969499.
87. Michielse, C.B.; Becker, M.; Heller, J.; Moraga, J.; Collado, I.G.; Tudzynski, P. The *Botrytis cinerea* Reg1 protein, a putative transcriptional regulator, is required for pathogenicity, conidiogenesis, and the production of secondary metabolites. *Mol. Plant-Microbe Interact.* **2011**, *24*, 1074–1085, doi:10.1094/MPMI-01-11-0007.
88. Schumacher, J.; Simon, A.; Cohrs, K.C.; Traeger, S.; Porquier, A.; Dalmais, B.; Viaud, M.; Tudzynski, B. The VELVET complex in the gray mold fungus *Botrytis cinerea*: Impact of BcLAE1 on differentiation, secondary metabolism, and virulence. *Mol. Plant-Microbe Interact.* **2015**, *28*, 659–674, doi:10.1094/MPMI-12-14-0411-R.
89. Schumacher, J.; Simon, A.; Cohrs, K.C.; Viaud, M.; Tudzynski, P. The Transcription factor BcLTF1 regulates virulence and light responses in the necrotrophic plant pathogen *Botrytis cinerea*. *PLoS Genet.* **2014**, *10*, e1004040, doi:10.1371/journal.pgen.1004040.
90. Udompaisarn, S.; Toopaang, W.; Sae-Ueng, U.; Srisuksam, C.; Wichienchote, N.; Wasuwan, R.; Nahar, N.A.S.; Tanticharoen, M.; Amnuaykanjanasin, A. The polyketide synthase PKS15 has a crucial role in cell wall formation in *Beauveria bassiana*. *Sci. Rep.* **2020**, *10*, 12630, doi:10.1038/s41598-020-69417-w.
91. Choquer, M.; Fournier, E.; Kunz, C.; Levis, C.; Pradier, J.-M.; Simon, A.; Viaud, M. *Botrytis cinerea* virulence factors: new insights into a necrotrophic and polyphageous pathogen. *FEMS Microbiol. Lett.* **2007**, *277*, 1–10, doi:10.1111/j.1574-6968.2007.00930.x.
92. de Vallée, A.; Bally, P.; Bruel, C.; Chandat, L.; Choquer, M.; Dieryckx, C.; Dupuy, J.W.; Kaiser, S.; Latorse, M.-P.; Loisel, E.; et al. A similar secretome disturbance as a hallmark of non-pathogenic *Botrytis cinerea* ATMT-mutants? *Front. Microbiol.* **2019**, *10*, doi:10.3389/fmicb.2019.02829.
93. Leisen, T.; Werner, J.; Pattar, P.; Safari, N.; Ymeri, E.; Sommer, F.; Schroda, M.; Suárez, I.; Collado, I.G.; Scheuring, D.; et al. Multiple knockout mutants reveal a high redundancy of phytotoxic compounds contributing to necrotrophic pathogenesis of *Botrytis cinerea*. *PLOS Pathog.* **2022**, *18*, e1010367, doi:10.1371/journal.ppat.1010367.

94. Rossi, F.R.; Gárriz, A.; Marina, M.; Romero, F.M.; Gonzalez, M.E.; Collado, I.G.; Pieckenstain, F.L. The sesquiterpene botrydial produced by *Botrytis cinerea* induces the hypersensitive response on plant tissues and its action is modulated by salicylic acid and jasmonic acid signaling. *Mol. Plant-Microbe Interact.* **2011**, *24*, 888–896, doi:10.1094/MPMI-10-10-0248.
95. Zhang, C.; He, Y.; Zhu, P.; Chen, L.; Wang, Y.; Ni, B.; Xu, L. Loss of bcbrn1 and bcpks13 in *Botrytis cinerea* not only blocks melanization but also increases vegetative growth and virulence. *Mol. Plant-Microbe Interact.* **2015**, *28*, 1091–1101, doi:10.1094/MPMI-04-15-0085-R.
96. Robert, X.; Gouet, P. Deciphering key features in protein structures with the new ENDscript server. *Nucleic Acids Res.* **2014**, *42*, W320–W324, doi:10.1093/nar/gku316.
97. Tamura, K.; Stecher, G.; Kumar, S. MEGA11: Molecular evolutionary genetics analysis version 11. *Mol. Biol. Evol.* **2021**, *38*, 3022–3027, doi:10.1093/molbev/msab120.
98. Jumper, J.; Evans, R.; Pritzel, A.; Green, T.; Figurnov, M.; Ronneberger, O.; Tunyasuvunakool, K.; Bates, R.; Žídek, A.; Potapenko, A.; et al. Highly accurate protein structure prediction with AlphaFold. *Nature* **2021**, *596*, 583–589, doi:10.1038/s41586-021-03819-2.
99. González-Rodríguez, V.E.; Garrido, C.; Cantoral, J.M.; Schumacher, J. The F-actin capping protein is required for hyphal growth and full virulence but is dispensable for septum formation in *Botrytis cinerea*. *Fungal Biol.* **2016**, *120*, 1225–1235, doi:10.1016/j.funbio.2016.07.007.
100. Mansfield, J.W. Fungal nutrition and physiology. *Physiol. Plant Pathol.* **1985**, *26*, 120, doi:10.1016/0048-4059(85)90036-0.
101. van der Vlugt-Bergmans, C.J.B.; Wagemakers, C.A.M.; van Kan, J.A.L. Cloning and expression of the cutinase A gene of *Botrytis cinerea*. *Mol. Plant-Microbe Interact.* **1997**, *10*, 21–29, doi:10.1094/MPMI.1997.10.1.21.
102. Schumacher, J. Tools for *Botrytis cinerea*: New expression vectors make the gray mold fungus more accessible to cell biology approaches. *Fungal Genet. Biol.* **2012**, *49*, 483–497, doi:10.1016/j.fgb.2012.03.005.
103. Colot, H. V.; Park, G.; Turner, G.E.; Ringelberg, C.; Crew, C.M.; Litvinkova, L.; Weiss, R.L.; Borkovich, K.A.; Dunlap, J.C. A high-throughput gene knockout procedure for *Neurospora* reveals functions for multiple transcription factors. *Proc. Natl. Acad. Sci.* **2006**, *103*, 10352–10357, doi:10.1073/pnas.0601456103.
104. Livak, K.J.; Schmittgen, T.D. Analysis of relative gene expression data using real-time quantitative PCR and the 2−ΔΔCT method. *Methods* **2001**, *25*, 402–408, doi:10.1006/meth.2001.1262.
105. Cui, K.; He, L.; Zhao, Y.; Mu, W.; Lin, J.; Liu, F. Comparative analysis of *Botrytis cinerea* in response to the microbial secondary metabolite benzothiazole using iTRAQ-based quantitative proteomics. *Phytopathology* **2021**, *111*, 1313–1326, doi:10.1094/PHYTO-11-20-0503-R.
106. Schneider, C.A.; Rasband, W.S.; Eliceiri, K.W. NIH Image to ImageJ: 25 years of image analysis. *Nat. Methods* **2012**, *9*, 671–675, doi:10.1038/nmeth.2089.
107. Sekulska-Nalewajko, J.; Gocławski, J.; Chojak-Koźniewska, J.; Kuźniak, E. Automated image analysis for quantification of reactive oxygen species in plant leaves. *Methods* **2016**, *109*, 114–122, doi:10.1016/j.ymeth.2016.05.018.